2019-06

Sea ice control on winter subsurface temperatures of the North Iceland Shelf during the Little Ice Age: A TEX_{86} calibration case study

David J. Harning [1, 2, 3 *], John T. Andrews [2], Simon T. Belt [4], Patricia Cabedo-Sanz [4], Nadia Dildar [2, 3], Áslaug Geirsdóttir [1], Gifford H. Miller [1, 2], Julio Sepúlveda [2, 3 *]

[1] Faculty of Earth Sciences, University of Iceland, Reykjavík, Iceland
[2] INSTAAR and Department of Geological Sciences, University of Colorado Boulder, Boulder, CO, USA
[3] Organic Geochemistry Laboratory, University of Colorado Boulder, Boulder, CO, USA
[4] Biogeochemistry Research Centre, School of Geography, Earth and Environmental Sciences, Plymouth University, Plymouth, UK

[*] Corresponding authors

David J. Harning and Julio Sepúlveda
Email: david.harning@colorado.edu; jsepulveda@colorado.edu

Journal: *Paleoceanography and Paleoclimatology*

Key Points:

1) Our local Icelandic GDGT calibration produces more realistic temperature estimates with substantially lower uncertainty over broader spatial calibrations
2) Periods of thick sea ice during the Little Ice Age likely warmed the subsurface as a result of winter insulation

Keywords: North Iceland Shelf, marine sediment, Little Ice Age, lipid biomarkers, IP_{25}, GDGTs

Abstract

Holocene paleoceanographic reconstructions along the North Iceland Shelf (NIS) have employed a variety of sea-surface temperature (SST) and sea-ice proxies. However, these surface proxies tend to have a seasonal bias toward spring/summer, and thus, only provide a discrete snapshot of surface conditions during one season. Furthermore, SST proxies can be influenced by additional confounding variables resulting in markedly different Holocene temperature reconstructions. Here, we expand Iceland's marine paleoclimate toolkit with TEX_{86}^{L}; a temperature proxy based on the distribution of archaeal glycerol dibiphytanyl glycerol tetraether (GDGT) lipids. We develop a local Icelandic calibration from 21 surface sediment samples covering a wide environmental gradient across Iceland's insular shelves. Locally calibrated GDGT results demonstrate that: 1) TEX_{86}^{L} reflects winter subsurface (0-200 m) temperatures on the NIS, and 2) our calibration produces more realistic temperature estimates with substantially lower uncertainty (S.E. ±4 ^{o}C) over global calibrations. We then apply this new calibration to a high-resolution marine sediment core (last millennium) collected from the central NIS (B997-316 GGC, 658 m depth) with age control constrained by ^{14}C-dated mollusks. To test the veracity of the GDGT subsurface temperatures, we analyze quartz and calcite wt% and a series of highly branched isoprenoid alkenes, including the sea ice biomarker IP_{25}, from the same core. The sediment records demonstrate that the development of thick sea ice during the Little Ice Age warmed the subsurface due to winter insulation. Importantly, this observation reflects a seasonal component of the sea-ice/ocean feedback to be considered for the non-linear cooling of the Little Ice Age in and around Iceland.

1. Introduction

The steep oceanographic (temperature, salinity, and nutrient) gradients caused by the presence of Arctic and Atlantic Ocean currents surrounding Iceland have made the insular shelves targets for northern North Atlantic climate change studies since the last deglaciation (Knudsen et al., 2004; Ólafsdóttir et al., 2010). Throughout the Holocene, the strength and latitudinal position of these currents has varied on centennial timescales, impacting terrestrial climate (Larsen et al., 2012; Geirsdóttir et al., 2013, 2019; Harning et al., 2018), as well as the status of Icelandic ice caps (Larsen et al., 2011; Brynjólfsson et al., 2015; Harning et al., 2016a, 2016b; Anderson et al., 2018). As the North Atlantic is the region that exhibits the largest meridional heat flux of the Northern Hemisphere (Wunsch, 1980), and the area of deep-water formation that drives the Atlantic Meridional Overturning Circulation (AMOC), changes in local climate also have widespread hemispheric relevance (Denton & Broecker, 2008; Buckley & Marshall, 2016). Thus, gaining a more comprehensive understanding of the past oceanographic conditions in this region of the North Atlantic is not only key to understanding past episodes of climate change, but also critical to contextualize circulation changes under a currently warming climate (Spielhagen et al., 2011; Caesar et al., 2018; Thornalley et al., 2018).

Over recent decades, numerous marine sediment core studies have generated surface and bottom water temperature proxy records based on Mg/Ca and $\delta^{18}O$ of benthic and planktic foraminifera, calcite wt%, the alkenone unsaturation index ($U_{37}^{k'}$) and biotic species assemblages, such as dinoflagellates and diatoms (Andersen et al., 2004; Castañeda et al., 2004; Giraudeau et al., 2004; Smith et al., 2005; Solignac et al., 2006; Bendle & Rosell-Melé, 2007; Justwan et al., 2008; Ran et al., 2008; Ólafsdóttir et al., 2010; Jiang et al., 2015; Moossen et al., 2015; Kristjánsdóttir et al., 2016). Sea surface temperature (SST)

93 proxies derived from phytoplankton result in a bias toward spring/summer SST and are
94 influenced by additional confounding variables (i.e., salinity, nutrients, and depth habitat
95 of biota, e.g., Prahl et al., 2006; Chival et al., 2014), resulting in markedly different
96 Holocene temperature reconstructions around Iceland (Kristjánsdóttir et al., 2016). As an
97 example, the Little Ice Age (LIA, 1250-1850 CE) is believed to be the coldest multi-
98 centennial climate anomaly of the Holocene in Iceland, yet the coldest Holocene conditions
99 inferred from alkenones (Kristjánsdóttir et al., 2016), dinocysts (Solignac et al., 2006) and
100 diatoms (Andersen et al., 2004; Justwan et al., 2008) occur earlier, between 4 and 2 ka.
101 Although the cooling observed in some proxies between 4 and 2 ka may be linked to long-
102 term changes in the AMOC (Hall et al., 2004) and/or North Atlantic Oscillation (Orme et
103 al., 2018), expanding Iceland’s quantitative proxy toolkit may help reconcile proxy
104 discrepancies.

105 In this study, we focus on quantifying the distribution of archaeal glycerol
106 dibiphytanyl glycerol tetraethers (GDGTs) archived in marine sediment from the North
107 Iceland Shelf (NIS). Although yet to be used to reconstruct marine paleoclimate on the
108 NIS, GDGT distributions have been shown to reflect modern winter subsurface
109 temperature (subT, 0-200 m) around Iceland (Rodrigo-Gámiz et al., 2015), the North Sea
110 (Herfort et al., 2006), Skagerrak (Rueda et al., 2009), and Antarctica (Kim et al., 2010,
111 2012). Assuming temperature is the dominant control on the distribution of GDGTs on the
112 NIS (Schouten et al., 2013 and references therein), but acknowledging that at least part of
113 the variability could also be explained by confounding effects such as ammonia oxidation
114 rates (Hurley et al., 2016), we improve absolute temperature estimates by developing a
115 local Icelandic calibration based on the analysis of surface sediments. We then apply this

local calibration to our late Holocene marine sediment core record. A suite of additional oceanographic surface climate proxies from the same core allow us to test the veracity of and to explore controls on GDGTs-based temperatures around Iceland.

2. Regional Setting

Today, the NIS represents the boundary where Arctic and Atlantic Ocean currents intercept (Fig. 1a-b, Stefánsson, 1962; Hopkins, 1991; Belkin et al., 2009). This front separates the cool, low salinity and sea-ice-bearing East Icelandic Current (EIC, 1 to 4 ^{o}C) to the north from the warmer and more saline Atlantic waters carried by the North Iceland Irminger Current (NIIC, 5 to 8 ^{o}C) on the inner and mid-shelf (Orvik et al., 2001). The current density differences between the two water masses result in vertical stratification along the NIS, such that the NIIC overlies the denser and cooler Upper Arctic Intermediate Waters (<0 ^{o}C, UAIW) (Fig. 1c). Within 70-100 km from Iceland’s northern coastline, freshwater run-off and summer heating modify the NIIC surface waters and form “coastal surface waters” (Fig. 1c), which then disintegrate during the following winter (Stefánsson, 1962; Ólafsson et al., 2008). The onset of this stratification in early spring triggers the spring bloom of phytoplankton (Zhai et al., 2012).

Atlantic waters provide the primary source of nutrients (i.e., phosphate, nitrate, silica) to the Icelandic shelves. Due to the greater influence of nutrient-deficient polar waters, NIS nutrient concentrations are considerably lower compared to those along the south of Iceland, where Atlantic waters dominate (Stefánsson, 1968; Stefánsson & Ólafsson, 1991). Although the freshwater run-off from Iceland is key for the seasonal stratification and phytoplankton blooms along the NIS, it has negligible direct effects on

nitrate and phosphate concentrations throughout the water column (Stefánsson & Ólafsson, 1991). In terms of modern oxygen saturation, the eastern NIS has similar values to those of waters south of Iceland, which may suggest relatively high rates of productivity for both locations (Stefánsson & Ólafsson, 1991). However, given that the NIS is rather limited in available nutrients, the relatively high oxygen saturation on the NIS may also relate to higher solubility of the colder Arctic waters.

Sea ice is also an integral component of the NIS. Iron oxide data on detrital grains suggest that drift ice is predominately sourced from east and southeast Greenland but also from as far as Canada and Russia, with the latter distal sources dramatically increasing in abundance over the last 1 ka (Andrews et al., 2009a; Darby et al., 2017). The presence of and correlation between quartz and the IP_{25} biomarker – proxies for sea ice extent - in core-top sediment along the NIS, and their absence from Iceland’s southern and western shelves further supports the dominance of drift ice origins over local sea ice production (Axford et al., 2011; Cabedo-Sanz et al., 2016a). When present, sea ice limits the exchange of heat, gases and moisture between the ocean and atmosphere, in addition to insulating the colder polar atmosphere from the relatively warmer ocean during winter (Thorndike et al., 1975; Maykut, 1978, 1982). Due to Iceland’s close proximity to the historical (post-1870 CE) sea ice edge (Divine & Dick, 2007), past changes in sea ice advection along the EIC have resulted in profound changes in local marine and terrestrial climate (Ogilvie & Jónsson, 2001; Moros et al., 2006; Massé et al., 2008; Miller et al., 2012; Cabedo-Sanz et al., 2016a).

3. Methods

3.1. Surface and marine core sediments

During July 1997, the cooperative USA/Icelandic *Bjarni Sæmundsson* B997 research cruise visited 30 locations across Iceland’s western and northern shelves (Helgadóttir, 1997). At each location, marine surface sediments were collected using a grab sampler. Previous studies have used these surface samples to describe the regional distributions of foraminifera $\delta^{18}O$ (Smith et al., 2005), quartz wt % (Andrews & Eberl, 2007), and the sea ice biomarker IP_{25} (Axford et al., 2011; Cabedo-Sanz et al., 2016a). We selected a subset (n=11) of these marine surface sediment samples for GDGT analyses to help construct a local Icelandic calibration (Fig. 1). As many of the 30 surface sediment locations were spatially clustered, our selection provides a representative sample from each geographical location the cruise covered, and, thus optimizes our local calibration by spanning the full range of oceanographic conditions present around Iceland today. The B997 cruise also recovered a suite of piston and gravity sediment cores. In this study, we focus on giant gravity core B997-316 GGC (2.47 m long) from the central North Iceland Shelf (66.75°N, 18.79°W, 658 mbsl, Fig. 1) (Helgadóttir, 1997). Sediment (~1 cm^3) was subsampled every six cm for minerological and biomarker analyses. In order to minimize the degradation of biomarkers (e.g., Cabedo-Sanz et al., 2016b), samples were taken from cores stored at 4 ^{o}C. All samples were subsequently freeze-dried and kept in the freezer (-20 ^{o}C) prior to biomarker extraction.

3.2. Age control

Four radiocarbon-based age control points are derived from a combination of mollusks (*T. equalis*) and benthic foraminifera (*N. labradorica* and *G. auriculata arctica*) sampled from the B997-316 GGC core (Table 1). As the B997-316 GGC core lacked datable material in

185 the uppermost sediment, two additional mollusks (*T. equalis*) were sampled from the near
186 surface sediment of an adjacent short gravity core, B997-316 SGC (Table 1), to confirm
187 that the tops of the sediment cores are modern and that no surface sediment was lost during
188 coring. Samples were prepared for AMS radiocarbon dating at the Institute of Arctic and
189 Alpine Research (INSTAAR) ^{14}C Preparation Lab and analyzed at the University of
190 California Irvine.
191
192 *3.3. Minerological analyses*
193 Quantitative X-ray diffraction (qXRD) analysis was conducted on the <2 mm sediment
194 fraction using the method developed by Eberl (2003) and used extensively on sediment
195 samples on other B997- cores (Andrews & Eberl, 2007; Andrews et al., 2009a; Andrews,
196 2009). Comparison between qXRD weight percent estimates on known mineral mixtures
197 and replicate analyses indicate that the errors on the weight percent estimates of both are
198 in the range of ±1 %. For B997-316 GGC, we focus on the identification of quartz as a
199 proxy to reconstruct the incursion of drift ice into Icelandic waters (i.e., sea ice and/or
200 icebergs), and calcite as a proxy of ocean productivity (Andrews et al., 2001).
201
202 *3.4. Biomarker analyses*
203 At the University of Plymouth, freeze-dried subsamples (~1-2 g) from core B997-316 GGC
204 were extracted for biomarkers by ultrasonication using dichloromethane:methanol (2:1,
205 v/v). Samples were initially spiked with an internal standard (9-octylheptadec-8-ene, 9-
206 OHD, 10 μL; 10 μg mL^{-1}) to permit quantification of highly branched isoprenoid (HBI)
207 alkenes. Total lipid extracts (TLEs) were separated into three fractions (F1-F3) using silica

column chromatography, after elution with hexane (6 mL), hexane:methylacetate (80:20, v/v, 6 mL), and methanol (4 mL), respectively. The F1 fraction contained aliphatic hydrocarbons including highly branched isoprenoids (HBIs; i.e., IP_{25}, $C_{25:2}$ and $C_{25:3}$), whereas F2 contained lipids with hydroxyl functional groups, including GDGTs. At the University of Colorado Boulder, freeze dried marine surface sediment samples (~3-7 g) were extracted three times on a Dionex accelerated solvent extractor (ASE 200) using dichloromethane:methanol (9:1, v/v) at 100 ºC and 2000 psi, and kept as TLEs for the GDGT analysis.

The IP_{25} ($C_{25:1}$), diene II ($C_{25:2}$) and triene Z ($C_{25:3}$) biomarkers were analyzed at the University of Plymouth as described by Belt et al. (2012, 2015). Analysis of the F1 was performed via gas chromatography-mass spectrometry (GC-MS) following the methods and operating conditions of Belt et al. (2012) on an Agilent 7890A GC coupled to a 5975 series mass selective detector fitted with an Agilent HP-5ms column (30 m x 0.25 mm x 0.25 mm). Mass spectrometric analyses were carried out in selected ion monitoring mode. The identification of IP_{25} (Belt et al., 2007), diene II (Belt et al., 2007) and triene Z (Belt et al., 2000) was based on their characteristic GC retention indices (RI_{HP5MS} = 2081, 2082, and 2044 for IP_{25}, diene II, and triene Z, respectively) and mass spectra (Belt, 2018). Quantification of lipids was achieved by comparison of mass spectral responses of selected ions (IP_{25}, *m/z* 350; diene II, *m/z* 348; triene Z, *m/z* 346) with those of the internal standard (9-OHD, *m/z* 350) and normalized according to their respective response factors and sediment masses (Belt et al., 2012). Analytical reproducibility was monitored using a standard sediment with known abundances of biomarkers for every 14-16 sediment samples extracted (analytical error 4%, n = 31).

For GDGTs, we analyzed aliquots of the F2 from B997-316 GGC and aliquots of the TLE from marine surface sediment samples in the Organic Geochemistry Laboratory at the University of Colorado Boulder. Dry samples were dissolved in hexane:isopropanol (99:1, v/v), sonicated, vortexed, and then filtered using a 0.45 μm PTFE syringe filter. Prior to analysis samples were spiked with 10 ng of the C_{46} GDGT internal standard (Huguet et al., 2006). Isoprenoid GDGTs were identified and quantified via high performance liquid chromatography – mass spectrometry (HPLC-MS) following modified methods of Hopmans et al. (2016) on a Thermo Scientific Ultimate 3000 HPLC interphased to a Q Exactive Focus Orbitrap-Quadrupole MS. Rather than starting at 18% hexane:isopropanol (9:1, v/v) (Hopmans et al., 2016), we began our eluent gradient with 30% hexane:isopropanol (9:1, v/v) to shorten retention and overall run times without compromising the chromotographic separation of GDGTs. The HPLC was conditioned for 20 minutes between runs. Samples were analyzed on full scan mode with a mass range of 500-1500 *m/z* at 70,000 mass resolution. GDGTs were identified based on their characteristic masses and elution patterns. We adopt the TEX_{86}^{L} index to reflect relative changes in temperature, which is a modification of the original TEX_{86} index (Schouten et al., 2002) constructed for temperatures <15 ºC (Kim et al., 2010, 2012):

$$TEX_{86}^{L} = \log\left(\frac{[GDGT-2]}{[GDGT-1]+[GDGT-2]+[GDGT-3]}\right)$$

3.5. Local Icelandic TEX_{86}^{L} calibration

The largest uncertainty in the temperature relationship of GDGTs in global calibrations is at the low end of the temperature spectrum (<5 ºC, Kim et al., 2010, 2012), which may reflect a reduced sensitivity of Thaumarchaeota to temperature in cooler climates (Wuchter

et al., 2004) or different regional oceanographic effects. Although a recent spatially-varying, Bayesian TEX_{86}-temperature calibration model was developed to capture regional oceanography variability (Tierney & Tingley, 2014), it excludes high-latitude settings and does not include any core top samples within a ~1000-km radius of Iceland. Hence, we targeted a network of local marine surface sediments (Fig. 1) to develop a local calibration that innately reflects the nuances of Icelandic oceanography and low local temperatures. We supplemented our 11 surface sediment samples with 10 previously published surface sediment samples from around Iceland (Table 2, Rodrigo-Gámiz et al., 2015) to generate a more comprehensive GDGT calibration that spans a larger geographical area and temperature gradient than obtainable using B997 samples alone. We note that although Rodrigo-Gámiz et al. (2015) sampled the surface of sediment cores, our samples were collected used a grab sampler, which may disturb the original sedimentary structure. However, natural factors such as sea floor mixing and variable sedimentation rates will always introduce uncertainty in the temperature embedded no matter how the sample is collected. Thus, we contend that the datasets can be merged for calibration purposes.

To calibrate the TEX_{86}^{L} index, *in situ* decadal mean temperatures from 1995-2004 CE were obtained from the World Ocean Atlas (WOA09, Locarnini et al., 2010) at the quarter-degree pixel where each surface sediment site is located. Subsequently, seasonal (spring, summer, fall, winter) and annual SST, in addition to 0-10 m, 0-20 m, 0-30 m, 0-40 m, 0-50 m, 0-60 m, 0-70 m, 0-80 m, 0-90 m, 0-100 m, 0-125 m, 0-150 m, 0-175 m, 0-200 m depth subsurface temperature integrations, were each regressed against the 21 core top TEX_{86}^{L} index values (Rodgrio-Gámiz et al., 2015; this study) to assess which portion

of the water column and which season the GDGT distributions most closely correspond to around Iceland. We calculated *p*-values for each regression to determine their significance.

4. Results and Interpretations

4.1. Age model

An age model for the B997-316 GGC sediment core was generated in the CLAM software using the Marine13 calibration curve (ΔR=0, Reimer et al., 2013) and a smooth spline regression over 1000 iterations (Blaauw, 2010). The calibrated benthic foraminifera date from 49.5 cm depth produced an age reversal in the initial model, and thus, was identified as an outlier and removed from the final age model (Fig. 2). The ~400-year difference between the calibrated age of the foraminifera and that estimated from the model may relate to changes in ΔR resulting from variable water masses (Eiríksson et al., 2004; Wanamaker et al., 2012). The two mollusks from the adjacent short gravity core (B997-316 SGC) both returned conventional ^{14}C ages ≤ 400 years (Table 1), confirming modern sediment at the core top of the SGC.

Based on several lines of reasoning, we argue that the modern ages of the SGC can be used to validate the extrapolation of the B997-316 GGC age model to the surface (Fig. 2). First, given that both cores were collected from the same location, we can exclude any impacts from geographic-dependent factors, such as variable sedimentation rates or oceanographic currents, that may cause the age-depth relationships to differ between the two cores. Second, coring-dependent factors can also be excluded as the two cores were collected in succession of each other using the same equipment (Helgadóttir, 1997). Even though coring operations can result in the loss of saturated or poorly consolidated surface

sediment, the identical coring techniques employed suggests that if the SGC captures modern surface sediment, so should the GGC.

Given that our age model only uses the three lowermost mollusks from the GGC and the uppermost mollusk samples from the adjacent SGC, increased age uncertainty undoubtedly exists where no datable material could be obtained (i.e., ~1400-2000 CE). However, we argue that our age estimates throughout the entire GGC core are reasonably strong. First, NIS sedimentation rate slopes only change significantly between deglacial/nonglacial periods (Andrews et al., 2002; Xiao et al., 2017) due to the presence/absence of the Icelandic Ice Sheet. Following the rapid demise of the Icelandic Ice Sheet ~15 thousand years ago (Norðdahl and Ingólfsson, 2015; Patton et al., 2017), sedimentation rates have remained linear across the NIS (Castañeda et al., 2004), consistent with the linearity of B997-316 GGC’s sedimentation rate over the last millennium (Fig. 2). Second, when our age model is applied to the proxy datasets (Fig. 3), the interpreted period of the Little Ice Age (LIA, see following section) is consistent with previous age ranges in Iceland that are derived from high-resolution and precisely-dated terrestrial archives (Geirsdóttir et al., 2009; Larsen et al., 2011, 2012).

4.2. Sediment core B997-316 GGC

4.2.1. Minerological analyses

In Icelandic waters, the two minerals quartz and calcite are qualitative indicators that reflect the incursion of drift ice (i.e., sea ice and/or icebergs) and marine surface productivity, respectively (Andrews et al., 2001, 2009a). In years when cold low-salinity Arctic water dominates, sea ice (% quartz) increases and surface productivity (% calcite) decreases due to the development of a well stratified water column. The opposite is seen in the proxies

during years characterized by warm and saline Atlantic waters, which reduces sea ice presence and mixes the water column resulting in higher productivity. Not surprisingly, % quartz and calcite generally show an inverse relationship over the last millennium in B997-316 GGC, which can be interpreted as the relative dominance of Arctic versus Atlantic waters at this location (Fig. 3a-b).

Percent quartz ranges from 1.4 to 2.7 %, whereas calcite ranges from 5.4 to 8.3 % (Fig. 3a-b). Recent analyses using mineral mixtures with known quartz wt % of 3.5 and 1.5 (Andrews et al., 2018) confirm that these small amounts of quartz can be correctly measured. Prior to ~1250 CE, quartz is relatively low, and calcite is the highest of the record, suggesting a dominance of warmer Atlantic waters at this time. Subsequently, quartz begins a gradual yet quasi-episodic rise towards its peak abundance at ~1900 CE. On the other hand, calcite appears to decline more sharply to lower values after ~1250 CE and remain relatively low through ~1900 CE, when it rises to levels near its pre-1250 CE state. Based on these two minerals, the period between 1250 and 1900 CE was likely characterized by cooler Arctic waters that favored the advection of drift ice, vertical stratification and lower surface productivity on the NIS. Following 1900 CE, the conditions reverted back to a dominance of warmer Atlantic waters that favored restricted sea drift transport and higher surface productivity (Fig. 3).

4.2.2. Highly-branched isoprenoid (HBI) alkenes

The analysis of the biomarker IP_{25} (Belt et al., 2007), a monounsaturated C_{25} HBI biosynthesized by Arctic sea ice diatoms (Belt et al., 2008; Brown et al., 2014), has gained recent traction as a novel proxy for spring/summer sea ice conditions around Iceland (Massé et al., 2008; Andrews et al., 2009b; Sicre et al., 2013; Cabedo-Sanz et al., 2016a;

346 Xiao et al., 2017). Although the IP_{25} biomarker is well-preserved in Arctic and sub-Arctic
347 marine sediment and routinely applied in paleo sea ice reconstructions as old as 5.3 Ma
348 (Stein et al., 2016), questions remain regarding its vertical transport, degradation processes,
349 and environmental controls (see reviews by Belt & Müller, 2013; Belt, 2018). Notably, the
350 interpretation of its presence (or lack thereof) can be ambiguous. IP_{25} below the limit of
351 detection has often been interpreted as reflecting either a lack of seasonal sea ice cover, or
352 permanent and thick sea ice that inhibits light penetration needed for sea ice diatoms to
353 photosynthesize and grow. However, this is likely an over-simplification of a broader range
354 of scenarios that result in absent IP_{25} (Belt, 2018). In any case, further information may be
355 obtained by the complementary analysis of certain open-water phytoplankton biomarkers
356 (i.e., brassicasterol or dinosterol, Müller et al., 2011).

357 Based on a distinctively heavy stable carbon isotopic composition, in addition to
358 similar concentration profiles to IP_{25} across Arctic marine surface sediment, the di-
359 unsaturated HBI diene II also has an Arctic sea ice diatom source (Belt et al., 2008; Cabedo-
360 Sanz et al., 2013; Brown et al., 2014), and is made by some Antarctic sea ice algae as well
361 (Belt et al., 2016). In contrast, a tri-unsaturated HBI (hereafter, triene Z) is biosynthesized
362 by certain open-water diatoms (Belt et al., 2000, 2008, 2015; Rowland et al., 2001), and
363 sources for the Arctic and Antarctic have recently been identified (Belt et al., 2017).
364 Importantly, the presence (or lack thereof) of triene Z, like certain phytoplankton sterols,
365 may help differentiate between open-water or thick sea ice conditions inferred from IP_{25}
366 and diene II in the Arctic (Cabedo-Sanz et al., 2013; Smik et al., 2016; Köseoğlu et al.,
367 2018). However, since sterols may also be derived from other (e.g., terrestrial) sources in

addition to sea ice algae (Huang & Meinschein, 1976; Volkman, 1986; Volkman et al., 1998; Belt et al., 2013, 2018), we limit our analysis here to triene Z only.

HBIs were detected in all downcore samples, with the exception of 96.5 cm depth (1509 CE), where no triene Z, diene II or IP_{25} were detected (Fig. 3c-e). Concentrations ranged from near detection up to 1.6 ng/g sediment for triene Z, up to 19 ng/g sediment for diene II, and up to 4 ng/g sediment for IP_{25}. Triene Z exhibited the highest concentrations prior to 1200 CE, while its abundance diminished to very low or undetectable between ~1200 and 1800 CE (Fig. 3c). Triene Z then rises to higher concentrations up through 2000 CE. The similar relative trends of diene II and IP_{25} concentrations suggest that both HBIs are likely sourced from sea ice algae around Iceland, similar to other Arctic (Brown et al., 2014) and Antarctic locations (Collins et al., 2013). Periods of synchronous reductions of diene II and IP_{25} concentrations occur at ~1170-1290 CE, 1450-1650 CE, and 1880 CE-present.

The similar overall trends between % calcite and triene Z abundance suggest that both proxies indicate temperate water surface productivity (Fig. 3b-c). Hence, in years where warmer Atlantic waters dominate, both % calcite and triene Z abundance increase, while the opposite trend dominates during years characterized by cooler Arctic waters. The detection of both IP_{25} and % quartz throughout the record suggests that sea ice has been a persistent feature at this location of the NIS over the last millennium, even during intervals when elevated % calcite and triene Z suggest an increased influence of warmer Atlantic waters. We interpret the reduction of diene II and IP_{25} at ~1170-1290 CE and 1880 CE-present to reflect diminished seasonal sea ice because of higher concentrations of triene Z

at the same time. In contrast, the reduction of diene II and IP_{25} from 1450-1650 CE likely reflects a period of thick, perennial sea ice as triene Z was mostly undetectable (Fig. 3c-e).

4.2.3. Glycerol dibiphytanyl glycerol tetraethers (GDGTs)

Changes in the degree of cyclization (number of cyclopentane moieties) in GDGTs have classically been interpreted to represent a physiological response of marine ammonia oxidizing Thaumarchaeota to changes in *in situ* temperature (e.g., Schouten et al., 2002). Thus, the TEX_{86} paleothermometer index has been empirically linked to annual or winter subT (0-200 m depth) in global data sets (Schouten et al., 2002; Kim et al., 2010, 2012). This presumption is supported by a recent study along a latitudinal transect in the western Atlantic Ocean, which demonstrated that the most likely water depths where GDGTs are produced from and exported to marine sediment is around 80-250 m (Hurley et al., 2018), similar to evidence for archaea abundance maxima at 200 m depths in the Pacific Ocean (Karner et al., 2001). Considering that Thaumarchaeota are chemolithoautotrophs that perform ammonia oxidation (conversion of NH_4^+ to NO_2^-), they are typically more abundant around the primary NO_2^- maximum near the base of the photic zone (Francis et al., 2005; Church et al., 2010; Hurley et al., 2018), and are thus most productive when there is minimized phytoplanktic competition over NH_4^+ (Schouten et al., 2013). In the case of the Arctic region, the latter occurs during the less productive winter months when photosynthesis for sea surface species is inhibited, which may explain the seasonal winter temperature bias of GDGTs previously observed in this region (Rodrigo-Gámiz et al., 2015). However, in addition to subT, recent studies have shown that several other environmental and geochemical factors can influence the degree of cyclization, such as growth phase (Elling et al., 2014), ammonia oxidation rates (Hurley et al., 2016), and

oxygen concentrations (Qin et al., 2015). In contrast to some other marine temperature proxies, such as the $\delta^{18}O$ of planktic foraminifera, GDGTs do not seem to be influenced by variations in salinity (Wuchter et al., 2004, 2005; Elling et al., 2015). Finally, GDGTs appear to be relatively resistant to oxic degradation (Schouten et al., 2004), and thus, likely reflect original living conditions once deposited in the sedimentary record.

GDGTs were present above the detection limits in all marine sediment core samples, and substantially increase in concentration at the core top (Supplement Fig S1). The calculated TEX_{86}^{L} index ranged from -0.71 to -0.63 (Fig. 3f). The record displays high variability and a rather constant first order trend towards the present, in addition to the occurrence of two intervals of substantial decreases in TEX_{86}^{L} values during 1350-1530 CE and 1745-1975 CE. Both periods are preceded by periods of relatively higher TEX_{86}^{L} values during 1110-1350 CE and 1530-1745 CE, respectively. A full paleoceanographic interpretation of the TEX_{86}^{L} results is provided in the discussion.

4.3. Local Icelandic TEX_{86}^{L} calibration

GDGTs were also detected and above detection limits in all B997 marine surface sediments samples (n=11, Supplemental Fig S2). TEX_{86}^{L} values of these samples ranged from -0.72 to -0.61 (Table 2). The 10 marine surface sediment samples from Rodrigo-Gámiz et al. (2015) span a greater geographical and environmental range around Iceland, and hence exhibit a greater range of TEX_{86}^{L} values (-0.71 to -0.49, Table 2). When we use the combined set of Icelandic marine surface sediment samples (n=21), the regression analysis demonstrates that the integration of winter temperatures from the top 200 m of the water column provides the best regression coefficients (R^2=0.73, $p<0.001$) compared to the

integration of other seasonal temperatures and the mean annual value (Figs. 4). Thus, sedimentary values around Iceland most likely represent winter subT that integrate a signal of the uppermost 200 m of the water column, consistent with the findings of Rodrigo-Gámiz et al. (2015).

5. Discussion

5.1. Local Icelandic TEX_{86}^{L} vs. regional Arctic calibration

If we supplement the combined Icelandic data set with more marine surface sediment samples from the greater northern North Atlantic region (Kim et al., 2010), the correlation coefficients of our winter subT (0-200 m) regression is substantially reduced (R^2 = 0.43 vs. 0.73, Supplemental Fig S3). This suggests that a local Icelandic calibration is optimal over larger regional calibrations, and perhaps, more accurately captures the nuances of local Icelandic oceanography. We hypothesize that the poorer performance of a more regional GDGT calibration for the North Atlantic region may relate to the inclusion of: 1) surface sediment samples from distal locations that feature different oceanographic environments than Iceland (e.g., Hudson Bay), and/or 2) samples from higher latitude (e.g., Svalbard and the Barents Sea) that are less “responsive” in terms of GDGT cyclization as they fall under the colder end of the spectrum in the global TEX_{86}^{L} calibration, which is characterized by a higher uncertainty and deviation from linearity (Kim et al., 2010). The standard error in our Icelandic winter subT calibration for 0-200 m (±0.4 ºC), is also an order of magnitude lower than the error derived from global low temperature calibrations (e.g., 4.0 ºC, Kim et al., 2010; 2.8 ºC, Kim et al., 2012). The reduced uncertainty achieved in our Icelandic calibration highlights the growing need for the continued development and application of

regional calibrations in future biomarker-based paleoclimate reconstructions (e.g., Kaiser et al., 2015; Foster et al., 2016; Russell et al., 2018). This is particularly important in areas where the temperature relationship of GDGTs deviates from the overall linear correlation observed in global calibrations (i.e., cold and warm regions).

Despite the reduced uncertainty compared to global calibrations, the regression coefficient for the Icelandic winter subT calibration (R^2=0.73) is comparatively lower than the global calibration (R^2=0.86-0.87; Kim et al., 2010, 2012). We hypothesize that the unconstrained confounding influence of ammonia-oxidation on the degree of GDGT cyclization (e.g., Hurley et al., 2016) may contribute to the scatter of our dataset (Fig. 4b). Although specific ammonia (NH_4^+) and nitrite (NO_2^-) information for this region is currently unavailable, reduced (enhanced) ammonia oxidation rates in the water column throughout the year would result in increased (decreased) degree of cyclization, thus yielding higher and lower temperatures, respectively (Hurley et al., 2016). If ammonia oxidation rates are driven by changes in ammonia supply and utilization (e.g., reduced nutrient availability in Arctic waters, or competition with phytoplankton), we cannot separate the influence of nutrient variability on the Icelandic TEX_{86}^L values with our current dataset. While oxygen availability has also been shown to influence the degree of cyclization in GDGTs (Qin et al., 2015), this factor is unlikely to affect the distribution of GDGTs around Iceland as these waters are relatively well-mixed and ventilated today (Stefánsson & Ólafsson, 1991), and presumably have been since the early Holocene (Kristjánsdóttir et al., 2016). With all known controlling factors considered, we suggest that our local TEX_{86}^L calibration improves the temperature estimates for Icelandic winter

subsurface waters. Future work in constraining the effects of ammonia-oxidation around Iceland would undoubtedly benefit the application of TEX_{86} on the NIS.

By applying temperature calibrations to our down core TEX_{86}^{L} record, our data reveal rapid and abrupt temperature variability on the NIS during the last millennium (Fig. 5). If the existing annual SST (Kim et al., 2010) and annual subT TEX_{86}^{L} calibrations developed for polar regions (Kim et al., 2012) are applied, the GDGT distributions suggest that subT fluctuated up to 5 ^{o}C over the course of decades. These observations are considerably higher than expected, especially given that they are comparable to the magnitude of SST changes observed in other NIS proxy records over the entire Holocene (e.g., Andersen et al., 2004; Bendle & Rosell-Melé, 2007; Jiang et al., 2015; Kristjánsdóttir et al., 2016). As originally hypothesized, this exercise demonstrates that global calibrations that feature greater uncertainty for low temperatures and that do not include sites proximal to Iceland are not appropriate for the NIS. In contrast, by applying our local winter subT calibration, the magnitude of estimated subT is not only reduced to ranges more comparable to other proxy records for the last millennium but, importantly, also captures the modern instrumental winter subT (within calibration uncertainty) at the B997-316 GGC site (4 ^{o}C, Fig. 5), further reinforcing the application of our local Icelandic TEX_{86}^{L} calibration.

5.2. NIS surface and subsurface climate variability during the Little Ice Age

The NIS represents one of the few global examples where paleo-IP_{25} abundance in marine cores has been calibrated against observational and documentary records (Massé et al., 2008; Andrews et al., 2009b). As a result, the variability of IP_{25} has been routinely applied

504 to marine sediment around Iceland as a robust indicator for seasonal sea ice (Massé et al.,
505 2008; Andrews et al., 2009b; Sicre et al., 2013; Cabedo-Sanz et al., 2016a). Similar to these
506 previous studies, IP_{25} concentrations in B997-316 GGC increase abruptly during the 13th
507 century, and with the exception of the period 1450-1650 CE, remain elevated until the 19th
508 century when concentrations begin to diminish (Fig. 6a). By employing statistical analyses
509 on IP_{25} abundances and 11 other marine climate proxy datasets from marine sediment core
510 MD99-2263, Andrews et al. (2009b) showed that a major regime shift in the marine climate
511 off NW Iceland commenced after 1200 CE, possibly linked to a strengthening high-
512 pressure ridge over Greenland in winter/spring that favored stronger north/northwesterly
513 winds and increased drift ice export to Iceland. Our mineral and HBI records consistently
514 reflect major shifts in surface conditions at a similar time and in the same direction (Fig.
515 3a-e), reinforcing the observed regime shift in marine climate, and increase of sea ice in
516 particular, during the 13th century (Bergthórsson, 1969; Ogilvie & Jónsson, 2001; Massé
517 et al., 2008; Andrews et al., 2009b; Sicre et al., 2013; Cabedo-Sanz et al., 2016a). The
518 consistency of our surface productivity and sea ice proxy records in reflecting the
519 established understanding of marine climate over the last millennium on the NIS supports
520 the fidelity of the B997-316 GGC marine sediment record, and therefore, the interpretation
521 of the GDGT record.

522 When the GDGT record is converted to winter subT, two pronounced centennial-
523 scale cold anomalies exhibit mean winter subT below the record average of 4.34 ^{o}C; at
524 1350-1530 CE (3.99 ^{o}C) and at 1745-1975 CE (4.19 ^{o}C). These two cold anomalies are
525 consistent with low surface productivity (% calcite and triene Z) and increased seasonal
526 sea ice (% quartz, diene II, IP_{25}), which suggest greater dominance of colder Arctic surface

527 waters between ~1250 and 1900 CE (Fig. 6a-b). In addition, alkenone-derived SST from
528 marine core MD99-2275 50 km to the east (Fig. 1a) document steady cooling throughout
529 this interval (Fig. 6c, Sicre et al., 2011), further supporting the presence of cool, Arctic
530 surface waters in the vicinity of B977-316 at this time. However, the timing for the onset
531 (1350 CE) and termination (1975 CE) of LIA cooling observed in the subsurface during
532 winter appears to lag that of the surface (1250 and 1900 CE, respectively) (Fig. 6). A
533 variety of model and data-based studies have demonstrated that the LIA was triggered by
534 a combination of sustained stratospheric volcanic sulfate injection (Zhong et al., 2010;
535 Miller et al., 2012; Sicre et al., 2013; Slawinska & Robock, 2018), low total solar irradiance
536 (Shindell et al., 2001) and changes in the North Atlantic Oscillation, one of the major
537 modes of internal climate variability in the North Atlantic (Trouet et al., 2009). On the NIS,
538 these radiative forcings directly impact the ocean surface, as manifested in the immediate
539 and abrupt increase in seasonal sea ice, reduced northward heat transport and suppression
540 of SSTs (Miller et al., 2012). The phase relationship between the B997-316 GGC surface
541 proxies and GDGTs suggests that it may have taken up to a century for the radiative forcing
542 in contact with the surface to propagate to the subsurface.

543 The subsurface warming observed between the two subsurface cold anomalies
544 (~1530-1745 CE, Fig. 6d) may suggest a reduced influence of the colder Arctic water mass
545 that generally characterized the LIA. However, similar to our surface proxies (Fig. 6a-b)
546 and the alkenone-derived SST from MD99-2275 (Fig. 6c), a local schlerochronological ^{14}C
547 record (ΔR_{shell}) constructed from mollusk shells reflects the continued dominance of older
548 Arctic waters in the benthos as well (Fig. 6e, Wanamaker et al., 2012). In fact, between
549 1450-1650 CE, the combination of our IP_{25} and triene Z datasets suggest thicker and more

permanent sea ice above the B997-316 site (Fig. 6a-b), an interpretation supported by additional LIA sea ice proxy (IP_{25} and quartz) records from the NIS (Massé et al., 2008; Andrews et al., 2009b; Cabedo-Sanz et al., 2016a). If thick sea ice conditions are maintained throughout the year, the insulating effects of sea ice would warm the subsurface waters during winter, as reflected by our GDGT record (Fig. 6d). The thickening of sea ice that we observe at 1450 CE coincides with the local intensification of LIA terrestrial cooling manifested in the synchronous advance of local Icelandic ice caps (Larsen et al., 2011; Harning et al., 2016a), and reduced Icelandic lake productivity (Geirsdóttir et al., 2013, 2019; Harning et al., 2018). A previous data-modeling comparison showed that this LIA intensification was likely forced by another episode of high stratospheric sulfate loading from explosive tropical volcanism and sustained by sea-ice/ocean feedbacks that reflected incoming solar radiation during summer (Miller et al., 2012). We suggest that the winter sea ice insulation may be another important component of the sea-ice/ocean feedback to consider in the non-linear nature of Little Ice Age cooling around Iceland.

Following the dissipation of thick sea ice conditions at 1650 CE, rising IP_{25} and triene Z concentrations suggest the return to seasonal sea ice conditions that favored the co-productivity of sea ice and open water algae at the B997-316 site (Fig. 6a-b). The change in sea ice conditions is the likely mechanism for the return of lower subT at 1745 CE, inferred from low GDGT temperature anomalies (Fig. 6d). We hypothesize that as the sea ice thinned out during spring months, possibly spurred by the previously stored subsurface heat, the winter ice pack would have also thinned accordingly. Consequently, a more open winter sea ice pack would have facilitated increased heat flux from the ocean to the colder overlying atmosphere, as reflected by the lower GDGT-based subsurface temperatures.

6. Conclusion

Consistent with the community's growing comprehension of GDGT-based temperature records at high latitudes, we show that archaeal isoprenoid GDGT distributions (TEX_{86}^{L}) around Iceland predominately reflect winter subsurface temperatures (0-200 m). Furthermore, by developing a local calibration based on a network of surface sediment samples, reconstructed NIS subsurface temperature estimates and uncertainty are improved upon those obtained from regional and global calibrations. Our TEX_{86}^{L} subsurface paleotemperature record from the NIS captures the cooling likely associated with the LIA (1250-1900 CE), as seen in additional surface proxies (sea ice and marine productivity) from the same sediment core. However, the LIA onset, intensification, and termination of the subsurface lags those changes of the surface, suggesting that it may have up to a century for changes at the surface to propagate to the subsurface during the late Holocene. We propose that the development of thick sea ice conditions during the intensification of the LIA around 1450 CE insulated the subsurface in winter, resulting in apparently warmer seasonal subsurface waters. This mechanism likely represents another seasonal component of the sea-ice/ocean feedback to be considered in the abrupt cooling manifested in and around Iceland during the LIA.

Acknowledgements

We kindly thank the caption, crew, and scientific staffs of the 1997 *Bjarni Sæmundsson* (B997) cruise for their considerable assistance in obtaining marine sediment cores and surface samples. The B997 cruise was principally supported by the Marine Research

Institute of Iceland, with the University of Colorado’s participation supported by NSF grant #ATM-9531397. Biomarker analyses were supported by internal CU funding awarded to JS and a grant from the CU Retired Faculty Association to JTA. DJH has been supported by an Icelandic Center for Research (RANNÍS) Doctoral Student Grant #163431051. PCS and STB acknowledge support from the RANNÍS Grant of Excellence #141573052 awarded to ÁG and GHM. We greatly appreciate comments from two anonymous reviewers and the editor (Stephen Barker) that improved the overall quality and clarity of the manuscript. All data can be found online through the PANGAEA Data Publisher.

References

Andersen, C., Koç, N., Jennings, A.E., & Andrews, J.T. (2004). Nonuniform response of the major surface currents in the Nordic Seas to insolation forcing: Implications for the Holocene climate variability. *Paleoceanography, 19,* 1-16.

Anderson, L.S., Flowers, G.E., Jarosch, A.H., Aðalgeirsdóttir, G.Th., Geirsdóttir, Á., Miller, G.H., Harning, D.J., Thorsteinsson, T., Magnússon, E., & Pálsson, F., (2018). Holocene glacier and climate variations in Vestfirðir, Iceland, from the modeling of Drangajökull ice cap. *Quaternary Science Reviews, 190,* 39-56.

Andrews, J.T. (2009). Seeking a Holocene drift ice proxy: non-clay mineral variations from the SW to N-central Iceland shelf: trends, regime shifts, and periodicities. *Journal of Quaternary Science, 24,* 664-676.

Andrews, J.T., Belt, S.T., Ólafsdóttir, S., Massé, G., & Vare, L.L. (2009b). Sea ice and marine climate variability for NW Iceland/Denmark Strait over the last 2000 cal. yr BP. *The Holocene, 19,* 775-784.

Andrews, J.T., Darby, D.A., Eberl, D.D., Jennings, A.E., Moros, M., & Ogilvie, A. (2009a). A robust multi-site Holocene history of drift ice off northern Iceland: Implications for North Atlantic climate. The Holocene 19, 71-78.

Andrews, J.T., & Eberl, D.D. (2007). Quantitative mineralogy of surface sediments on the Iceland shelf, and application to down-core studies of Holocene ice-rafted sediments. *Journal of Sedimentary Research, 77,* 469-479.

Andrews, J.T., Hardardóttir, J., Geirsdóttir, Á., Helgadóttir, G., (2002). Late Quaternary ice extent and glacial history from the Djúpáll trough, off Vestfirdir peninsula, north-west Iceland: a stacked 36 cal. Ky environmental record. *Polar Research, 21,* 211-226.

Andrews, J.T., Helgadottir, G., Geirsdottir, Á., & Jennings, A.E. (2001). Multicentury-scale records of carbonate (hydrographic?) variability on the N. Iceland margin over the last 5000 yrs. *Quaternary Research, 56,* 199-206.

Andrews, J.T., Jónsdóttir, I., & Geirsdóttir, Á. (**2018**). Tracking Holocene drift-ice limits on the NW/SW Iceland shelf: comparing proxy data with observation and historical evidence. *Arctic, Antarctic, and Alpine Research, **in press***.

Axford, Y., Andresen, C.S., Andrews, J.T., Belt, S.T., Geirsdóttir, Á., Massé, G., Miller, G.H., Ólafsdóttir, S., & Vare, L.L. (2011). Do paleoclimate proxies agree? A test comparing 19 late Holocene climate and sea-ice reconstructions from Icelandic marine and lake sediments. *Journal of Quaternary Science, 26,* 645-656.

Belkin, I.M., Cornillon, P.C., & Sherman, K. (2009). Fronts in large marine ecosystems. *Progress in Oceanography, 81,* 223-236.

Belt, S.T. (2018). Source-specific biomarkers as proxies for Arctic and Antarctic sea ice. *Organic Geochemistry, 125,* 277–298.

Belt, S.T., Allard, W.G., Massé, G., Robert, J.-M., & Rowland, S.J. (2000). Highly branched isoprenoids (HBIs): Identification of the most common and abundant sedimentary isomers. *Geochimica and Cosmochimica Acta, 64,* 3839-3851.

Belt, S.T., Brown, T.A., Navarro Rodriguez, A., Cabedo Sanz, P., Tonkin, A., & Ingle, R. (2012). A reproducible method for the extraction, identification and quanitification of the Arctic sea ice proxy IP_{25} from marine sediments. *Analytical Methods, 4,* 704-713.

Belt, S.T., Brown, T.A., Smik, L., Assmy, P., & Mundy, C.J. (2018). Sterol identification in floating Arctic sea ice algal aggregates and the Antarctic sea ice diatom *Berkeleya adeliensis*. *Organic Geochemistry, 118,* 1-3.

Belt, S.T., Brown, T.A., Smik, L., Tatarek, A., Wiktor, J., Stowasser, G., Assmy, P., Allen, C.S., & Husum, K. (2017). Identification of C_{25} highly branched isoprenoid (HBI) alkenes in diatoms of the genus *Rhizosolenia* in polar and sub-polar marine phytoplankton. *Organic Geochemistry, 110,* 65–72.

Belt, S.T., Brown, T.A., Ringrose, A.E., Cabedo-Sanz, P., Mundy, C.J., Gosselin, M., & Poulin, M. (2013). Quantitative measurement of the sea ice diatom biomarker IP_{25} and sterols in Arctic sea ice and underlying sediments: Further considerations for palaeo sea ice reconstructions. *Organic Geochemistry, 62,* 33-45.

677 Belt, S.T., Cabedo-Sanz, P., Smik, L., Navarro-Rodriguez, A., Berben, S.M.P., Knies, J.,
678 & Husum, K. (2015). Identification of paleo Arctic winter sea ice limits and the marginal
679 ice zone: Optimised biomarker-based reconstructions of late Quaternary Arctic sea ice.
680 *Earth and Planetary Science Letters, 431*, 127-139.
681
682 Belt, S.T., Massé, G., Rowland, S.J., Poulin, M., Michel, C., & LeBlanc, B. (2007). A novel
683 chemical fossil of palaeo sea ice: IP_{25}. *Organic Geochemistry, 38*, 16-27.
684
685 Belt, S.T., Massé, G., Vare, L.L., Rowland, S.J., Poulin, M., Sicre, M.-A., Sampei, M., &
686 Fortier, L. (2008). Distinctive ^{13}C isotopic signature distinguishes a novel sea ice biomarker
687 in Arctic sediments and sediment traps. *Marine Chemistry, 112*, 158-167.
688
689 Belt, S.T., & Müller, J. (2013). The Arctic sea ice biomarker IP_{25}: a review of current
690 understanding, recommendations for future research and applications in palaeo sea ice
691 reconstructions. *Quaternary Science Reviews, 79*, 9-25.
692
693 Belt, S.T., Smik, L., Brown, T.A., Kim, J.-H., Rowland, S.J., Allen, C.S., Gal, J.-K., Shin,
694 K.-H., Lee, J.I., & Taylor, K.W.R. (2016). Source identification and distribution reveals
695 the potential of the geochemical Antarctic sea ice proxy $IPSO_{25}$. *Nature Communications,*
696 *7*, 1-10.
697
698 Bendle, J.A.P., & Rosell-Melé, A. (2007). High-resolution alkenone sea surface
699 temperature variability on the North Icelandic Shelf: implications for Nordic Seas
700 palaeoclimatic development during the Holocene. *The Holocene, 17*, 9-24.
701
702 Bergthórsson, P. (1969). An estimate of drift ice and temperature in Iceland in 1000 years.
703 *Jökull, 19*, 94-101.
704
705 Blaauw, M. (2010). Methods and code for 'classical' age-modeling of radiocarbon
706 sequences. *Quaternary Geochronology, 5*, 512-518.
707
708 Brown, T.A., Belt, S.T., Tatarek, A., & Mundy, C.J. (2014). Source identification of the
709 Arctic sea ice proxy IP_{25}. *Nature Communications, 5*, 4197.
710
711 Brynjólfsson, S., Schomacker, A., Ingólfsson, Ó., & Keiding, J.K. (2015a). Cosmogenic
712 ^{36}Cl exposure ages reveal a 9.3 ka BP glacier advance and the Late Weichselian-Early
713 Holocene glacial history of the Drangajökull region, northwest Iceland. *Quaternary*
714 *Science Reviews, 126*, 140-157.
715
716 Buckley, M.W., & Marshall, J. (2016). Observations, inferences, and mechanisms of the
717 Atlantic Meridional Overturning Circulation: A review. *Journal of Geophysics, 54*, 5-63.
718
719 Cabedo-Sanz, P., Belt, S.T., Jennings, A.E., Andrews, J.T., & Geirsdóttir, Á. (2016a).
720 Variability in drift ice export from the Arctic Ocean to the North Icelandic Shelf over the
721 last 8000 years: A multi-proxy evaluation. *Quaternary Science Reviews, 146*, 99-115.
722

723 Cabedo-Sanz, P., Belt, S.T., Knies, J., & Husum, K. (2013). Identification of contrasting
724 seasonal sea ice conditions during the Younger Dryas. *Quaternary Science Reviews, 79*,
725 74-86.
726
727 Cabedo-Sanz, P., Smik, L., & Belt, S.T. (2016b). On the stability of various highly
728 branched isoprenoid (HBI) lipids in stored sediments and sediment extracts. Organic
729 *Geochemistry*, *97*, 74-77.
730
731 Caesar, L., Rahmstorf, S., Robinson, A., Feulner, G., & Saba, V. (2018). Observed
732 fingerprint of a weakening Atlantic Ocean overturning circulation. *Nature*, *556*, 191-198.
733
734 Castañeda, I.S., Smith, L.M., Kristjánsdóttir, G.B., & Andrews, J.T. (2004). Temporal
735 changes in Holocene $\delta^{18}O$ records from northwest and central North Iceland Shelf. *Journal*
736 *of Quaternary Science*, *19*, 321-334.
737
738 Chivall, D., M'Boule, D., Sinke-Schoen, D., Sinninghe Damsté, J.S., Schouten, S., & van
739 der Meer, M.T.J. (2014). Impact of salinity and growth phase on alkenone distributions in
740 coastal haptophytes. *Organic Geochemistry, 67*, 31-34.
741
742 Church, M.J., Wai, B., Karl, D.M., & DeLong, E.F. (2010). Abundances of crenarchaeal
743 amoA genes and transcripts in the Pacific Ocean. *Environmental Microbiology, 12*, 679-
744 688.
745
746 Collins, L.G., Allen, C.S., Pike, J., Hodgson, D.A., Weckström, K., & Massé, G. (2013).
747 Evaluating highly branched isoprenoid (HBI) biomarkers as a novel Antarctic sea-ice
748 proxy in deep ocean glacial age sediments. *Quaternary Science Reviews, 79*, 87-98.
749
750 Darby, D.A., Andrews, J.T., Belt, S.T., Jennings, A.E., & Cabedo-Sanz, P. (2017).
751 Holocene cyclic records of ice-rafted debris and sea ice variations on the East Greenland
752 and Northwest Iceland margins. *Arctic, Antarctic, and Alpine Research, 49*, 649-672.
753
754 Denton, G.H., & Broecker, W.S. (2008). Wobbly ocean conveyor circulation during the
755 Holocene? *Quaternary Science Reviews*, *27*, 1939-1950.
756
757 Divine, D.V., & Dick, C. (2007). March through August Ice Edge Positions in the Nordic
758 Seas, 1750-2002, Version 1. Boulder, Colorado USA. *NSIDC: National Snow and Ice Data*
759 *Center*.
760
761 Eberl, D.D. (2003). *User guide to RockJock: A program for determining quantitative*
762 *mineralogy from X-ray diffraction data*. United States Geological Survey, Open File
763 Report 03-78, 40 pp, Washington, DC.
764
765 Eiríksson, J., Larsen, G., Knudsen, K.L., Heinemeier, J., & Símonarson, L.A. (2004).
766 Marine reservoir age variability and water mass distribution in the Iceland Sea. *Quaternary*
767 *Science Reviews, 23*, 2247-2268.
768

769 Elling, F.J., Könneke, M., Lipp, J.S., Becker, K.W., Gagen, E.J., & Hinrichs, K.-U. (2014).
770 Effects of growth phase on the membrane lipid composition of the thaumarchaeon
771 *Nitrosopumilus maritimus* and their implications for archaeal lipid distributions in the
772 marine environment. *Geochimica et Cosmochimica Acta, 141*, 579-597.
773
774 Elling, F.J., Könneke, M., Mußmann, M., Greve, A., & Hinrichs, K.-U. (2015). Influence
775 of temperature, pH, and salinity on membrane lipid composition and TEX_{86} of marine
776 planktonic thaumarchaeal isolates. *Geochimica et Cosmochimica Acta, 171*, 238-255.
777
778 Foster, L.C., Pearson, E.J., Juggins, S., Hodgson, D.A., Saunders, K.M., Verleyen, E., &
779 Roberts, S.J. (2016). Development of a regional glycerol dialkyl glycerol tetraether
780 (GDGT)-temperature calibration for Antarctic and sub-Antarctic lakes. *Earth and*
781 *Planetary Science Letters, 433*, 370-379.
782
783 Francis, C.A., Roberts, K.J., Beman, J.M., Santoro, A.E., & Oakley, B.B. (2005). Ubiquity
784 and diversity of ammonia-oxidizing archaea in water columns and sediments of the ocean.
785 *Proceedings of the National Academy of Sciences, 102*, 14683-14688.
786
787 Geirsdóttir, Á., Miller, G.H., Andrews, J.T., Harning, D.J., Anderson, L.S., Larsen, D.J.,
788 Florian, C. & Thordarson, T. (2019). The onset of Neoglaciation in Iceland and the 4.2 ka
789 event. *Climate of the Past Discussions, 14*, 25-40.
790
791 Geirsdóttir, Á., Miller, G.H., Larsen, D.J., & Ólafsdóttir, S. (2013). Abrupt Holocene
792 climate transitions in the northern North Atlantic region recorded by synchronized
793 lacustrine records in Iceland. *Quaternary Science Reviews, 70*, 48-62.
794
795 Geirsdóttir, Á., Miller, G.H., Thordarson, T., & Ólafsdóttir, K.B. (2009). A 2000 year
796 record of climate variations reconstructed from Haukadalsvatn, West Iceland. *Journal of*
797 *Paleolimnology, 41*, 95-115.
798
799 Giraudeau, J., Jennings, A.E., & Andrews, J.T. (2004). Timing and mechanisms of surface
800 and intermediate water circulation changes in the Nordic Sea over the last 10000 cal years:
801 A view from the North Iceland Shelf. *Quaternary Science Reviews, 23*, 2127-2139.
802
803 Hall, I.R., Bianchi, G.G., & Evans, J.R. (2004). Centennial to millennial scale Holocene
804 climate-deep water linkage in the North Atlantic. *Quaternary Science Reviews, 23*, 1529-
805 1536.
806
807 Harning, D.J., Geirsdóttir, Á., Miller, G.H., & Anderson, L. (2016a). Episodic expansion
808 of Drangajökull, Vestfirðir, Iceland over the last 3 ka culminating in its maximum
809 dimension during the Little Ice Age. *Quaternary Science Reviews, 152*, 118-131.
810
811 Harning, D.J., Geirsdóttir, Á., Miller, G.H., & Zalzal, K. (2016b). Early Holocene
812 deglaciation of Drangajökull, Vestfirðir, Iceland. *Quaternary Science Reviews, 153*, 192-
813 198.
814

Harning, D.J., Geirsdóttir, Á., & Miller, G.H. (2018). Punctuated Holocene climate of Vestfirðir, Iceland, linked to internal/external variables and oceanographic conditions. *Quaternary Science Reviews, 189*, 31-42.

Helgadóttir, G. (1997). Paleoclimate (0 to >14 ka) of W and NW Iceland: an Iceland/USA contribution to P.A.L.E. Cruise Report B9-97 R/V Bjarni Sæmundsson RE 30 17th-30th July 1997. *No. 62, Marine Research Institute of Iceland*, Reykjavík, Iceland.

Herfort, L., Schouten, S., Boon, J.P., & Sinninghe Damsté, J.S. (2006). Application of TEX_{86} temperature proxy to the southern North Sea. *Organic Geochemistry, 37*, 1715-1726.

Hopkins, T.S. (1991). The GIN Sea – A synthesis of its physical oceanography and literature review 1972-1985. *Earth Science Reviews, 30*, 175-318.

Hopmans, E.C., Schouten, S., & Sinninghe Damsté, J.S. (2016). The effect of improved chromatography on GDGT-based palaeoproxies. *Organic Geochemistry, 93*, 1-6.

Huang, W.-Y., & Meinschein, W. (1976). Sterols as ecological indicators. *Geochimica et Cosmochimica Acta, 43*, 739-745.

Huguet, C., Hopmans, E.C., Febo-Ayala, W., Thompson, D.H., Sinninghe Damsté, J.S., & Schouten, S. (2006). An improved method to determine the absolute abundance of glycerol dibiphytanyl glycerol tetraether lipids. *Organic Geochemistry, 37*, 1036-1041.

Hurley, S.J., Elling, F.J., Könneke, M., Buchwald, C., Wankel, S.D., Santoro, A.E., Lipp, J.S., Hinrichs, K.-U., & Pearson, A. (2016). Influence of ammonia oxidation rate on thaumarchaeal lipid composition and the TEX_{86} temperature proxy. *Proceedings of the National Academy of Sciences, 113*, 7762-7767.

Hurley, S.J., Lipp, J.S., Close, H.G., Hinrichs, K.-U., & Pearson, A. (2018). Distribution and export of isoprenoid tetraether lipids in suspended particulate matter from the water column of the Western Atlantic Ocean. *Organic Geochemistry, 116*, 90-102.

Jiang, H., Muscheler, R., Björck, S., Seidenkrantz, M.-S., Olsen, J., Sha, L., Sjolte, J., Eiríksson, J., Ran., L., Knudsen, K.-L., & Knudsen, M.F. (2015). Solar forcing of Holocene summer sea-surface temperatures in the northern North Atlantic. *Geology, 43*, 2-5.

Justwan, A., Koc, N., & Jennings, A.E. (2008). Evolution of the Irminger and East Icelandic Current systems through the Holocene, revealed by diatom-based sea surface temperature reconstructions. *Quaternary Science Reviews, 27*, 1571-1582.

Kaiser, J., Schouten, S., Kilian, R., Arz, H.W., Lamy, F., & Sinninghe Damsté, J.S. (2015). Isoprenoid and branched GDGT-based proxies for surface sediments from marine, fjord and lake environments in Chile. *Organic Geochemistry, 89-90*, 117-127.

Karner, M.B., DeLong, E.F., & Karl, D.M. (2001). Archaeal dominance in the mesopelagic zone of the Pacific Ocean. *Nature, 409*, 507-510.

Kim, J.-H., van der Meer, J., Schouten, S., Helmke, P., Willmott, V., Sangiorgi, F., Koç, N., Hopmans, E. C., & Sinninghe Damsté, J. S. (2010). New indices and calibrations derived from the distribution of crenarchaeal isoprenoid tetraether lipids: Implications for past sea surface temperature reconstructions. *Geochimica et Cosmochimica Acta*, *74*, 4639–4654.

Kim, J.-H., Crosta, X., Willmott, V., Renssen, H., Bonnin, J., Helmke, P., Schouten, S., & Sinninghe Damsté, J.S. (2012). Holocene subsurface temperature variability in the eastern Antarctic continental margin. *Geophysical Research Letters*, *39*, 3-8.

Knudsen, K.L., Eirikson, J., Jansen, E., Jiang, H., Rytter, F., & Gudmundsdottir, E.R. (2004). Paleoceanographic changes off North Iceland through the last 1200 yrs: foraminifera, stable isotopes, diatomes and ice rafted debris. *Quaternary Science Reviews*, *23*, 2231-2246.

Köseoğlu, D., Belt, S.T., Smik, L., Yao, H., Panieri, G., & Knies, J. (2018). Complementary biomarker-based methods for characterizing Arctic sea ice conditions: A case study comparison between multivariate analysis and the PIP_{25} index. *Geochimica et Cosmochimica Acta, 222*, 406-420.

Kristjánsdóttir, G.B., Moros, M., Andrews, J.T., & Jennings, A.E. (2016). Holocene Mg/Ca, alkenones, and light stable isotope measurements on the outer North Iceland shelf (MD99-2269): A comparison with other multi-proxy data and sub-division of the Holocene. *The Holocene*, *26*, 1-11.

Larsen, D.J., Miller, G.H., Geirsdóttir, Á., & Thordarson, T. (2011). A 3000-year varved record of glacier activity and climate change from the proglacial lake Hvítárvatn, Iceland. *Quaternary Science Reviews, 30*, 2715-2731.

Larsen, D.J., Miller, G.H., Geirsdóttir, Á., & Ólafsdóttir, S. (2012). Non-linear Holocene climate evolution in the North Atlantic: a high-resolution, multi-proxy record of glacier activity and environmental change from Hvítárvatn, central Iceland. *Quaternary Science Reviews, 39*, 14-25.

Locarnini, R.A., Mishonov, A.V., Antonov, J.I., Boyer, T.P., Garcia, H.E., Baranova, O.K., Zweng, M.M., & Johnson, D.R. (2010). *World Ocean Atlas 2009, Volume 1: Temperature*. S. Levitus, Ed. NOAA Atlas NESDIS 68, U.S. Government Printing Office, Washington, D.C., 184 pp.

Massé, G., Rowland, S.J., Sicre, M.-A., Jacob, J., Jansen, E., & Belt, S.T. (2008). Abrupt climate changes for Iceland during the last millenium: Evidence form high resolution sea ice reconstructions. *Earth and Planetary Science Letters, 269*, 565-569.

907 Maykut, G.A. (1978). Energy exchange over young sea ice in the central Arctic. *Journal*
908 *of Geophysical Research, 83*, 3646-3658.
909
910 Maykut, G.A. (1982). Large-scale heat exchange and ice production in the central Arctic.
911 *Journal of Geophysical Research, 87*, 7971-7984.
912
913 Miller, G.H., Geirsdóttir, Á., Zhong, Y., Larsen, D.J., Otto-Bliesner, B.L., Holland, M.M.,
914 Bailey, D.A., Refsnider, K.A., Lehman, S.J., Southon, J.R., Anderson, C., Björnsson, H.,
915 & Thordarson, T. (2012). Abrupt onset of the Little Ice Age triggered by volcanism and
916 sustained by sea-ice/ocean feedbacks. *Geophysical Research Letters, 39*, 1-5.
917
918 Moossen, H., Bendle, J., Seki, O., Quillmann, U., & Kawamura, K. (2015). North Atlantic
919 Holocene climate evolution recorded by high-resolution terrestrial and marine biomarker
920 records. *Quaternary Science Reviews, 129*, 111-127.
921
922 Moros, M., Andrews, J.T., Eberl, D.D., & Jansen, E. (2006). Holocene history of drift ice
923 in the northern North Atlantic: Evidence for differential spatial and temporal modes.
924 *Paleoceanography, 21*, 1-10.
925
926 Müller, J., Wagner, A., Fahl, K., Stein, R., Prange, M., & Lohmann, G. (2011). Towards
927 quantitative sea ice reconstructions in the northern North Atlantic: a combined biomarker
928 and numerical modelling approach. *Earth and Planetary Science Letters, 306*, 137-148.
929
930 Norðdahl, H., Ingólfsson, Ó., (2015). Collapse of the Icelandic ice sheet controlled by sea-
931 level rise? *Arktos, 13*, 1-18.
932
933 Ogilvie, A.E.J., & Jónsson, T. (2001). “Little Ice Age” research: A perspective from
934 Iceland. *Climatic Change, 48*, 9-52.
935
936 Ólafsdóttir, S., Jennings, A.E., Geirsdóttir, Á., Andrews, J., & Miller, G.H. (2010).
937 Holocene variability of the North Atlantic Irminger current on the south- and northwest
938 shelf of Iceland. *Marine micropaleontology, 77*, 101-118.
939
940 Ólafsson, J., Ólafsdóttir, S.R., & Briem, J. (2008). Vatnsföll og vistkerfi strandsjávar.
941 *Náttúrufræðingurinn, 76*, 95-108.
942
943 Orme, L.C., Miettinen, A., Divine, D., Husum, K., Pearce, C., Van Nieuwenhove, N., Born,
944 A., Mohan, R., & Seidenkrantz, M.-S. (2018). Subpolar North Atlantic sea surface
945 temperature since 6 ka BP: Indications of anomalous ocean-atmosphere interactions at 4-2
946 ka BP. *Quaternary Science Reviews, 194*, 128-142.
947
948 Orvik, K.A., Skagseth, Ø., & Mork, M. (2001). Atlantic inflow to the Nordic Seas: current
949 structure and volume fluxes from moored current meters, VM-ADCP and SeaSoar-CTD
950 observations, 1995-1999. *Deep-Sea Research, 48*, 937-957.
951

952 Patton, H., Hubbard, A., Bradwell, T., Schomacker, A., (2017). The configuration,
953 sensitivity and rapid retreat of the Late Weichselian Icelandic ice sheet. *Earth-Science*
954 *Reviews, 166*, 223-245.
955
956 Prahl, F.G., Mix, A.C., & Sparrow, M.A. (2006). Alkenone paleothermometry: Biological
957 lessons from marine sediment records off western South America. *Geochimica et*
958 *Cosmochimica Acta, 70*, 101-117.
959
960 Qin, W., Carlson, L.T., Armbrust, E.V., Devol, A.H., Moffett, J.W., Stahl, D.A., & Ingalls,
961 A.E. (2015). Confounding effects of oxygen and temperature on the TEX_{86} signature of
962 marine Thaumarchaeota. *Proceedings of the National Academy of Sciences, 112*, 10979-
963 10984.
964
965 Ran, L., Knudsen, K.L., & Eiríksson, J. (2008). A high-resolution Holocene diatom record
966 on the North Icelandic Shelf. *Boreas, 37*, 399-413.
967
968 Reimer, P.J., Bard, E., Bayliss, A., Beck, W.J., Blackwell, P.G., Brock Ramsey, C., Buck,
969 C.E., Cheng, H., Edwards, R.L., Friedrich, M., Grootes, P.M., Guilderson, T.P.,
970 Haflidason, H., Hajdas, I., Hatté, C., Heaton, T.J., Hoffmann, D.L., Hogg, A.G., Hughen,
971 K.A., Kaiser, K.F., Kromer, B., Manning, S.W., Niu, M., Reimer, R.W., Richards, D.A.,
972 Scott, E.M., Southon, J.R., Staff, R.A., Turney, C.S.M., & van der Plicht, J. (2013).
973 Intcal13 and Marine13 radiocarbon age calibration curves 0-50,000 years cal BP.
974 *Radiocarbon, 55*, 1869-1887.
975
976 Rodrigo-Gámiz, M., Rampen, S.W., de Haas, H., Baas, M., Schouten, S., & Sinninghe-
977 Damsté, J.S. (2015). Constraints on the applicability of the organic temperature proxies
978 Uk37´, TEX_{86} and LDI in the subpolar region around Iceland. *Biogeosciences, 12*, 6573-
979 6590.
980
981 Rowland, S.J., Allard, W.G., Belt, S.T., Massé, G., Robert, J.-M., Blackburn, S., Frampton,
982 D., Revill, A.T., & Volkman, J.K. (2001). Factors influencing the distributions of
983 polyunsaturated terpenoids in the diatom, *Rhizosolenia setigera*. *Phytochemistry, 58*, 717-
984 728.
985
986 Rueda, G., Rosell-Melé, A., Escala, M., Gyllencreutz, R., & Backman, J. (2009).
987 Comparison of instrumental and GDGT-based estimates of sea surface and air temperatures
988 from the Skaggerak. *Organic Geochemistry, 40*, 287-291.
989
990 Russell, J.M., Hopmans, E.C., Loomis, S.E., Liang, J., & Sinninghe Damsté, J.S. (2018).
991 Distributions of 5- and 6-methyl branched glycerol dialkyl glycerol tetraethers (brGDGTs)
992 in East African lake sediment: Effects of temperature, pH, and new lacustrine
993 paleotemperature calibrations. *Organic Geochemistry, 117*, 56-69.
994
995 Schouten, S., Hopmans, E.C., Schefuss, E., & Sinninghe Damsté, J.S. (2002).
996 Distributional variations in marine crenarchaeotal membrane lipids: a new tool for

reconstructing ancient sea water temperatures? *Earth and Planetary Science Letters, 204*, 265-274.

Schouten, S., Hopmans, E.C., & Sinninghe Damsté, J.S. (2004). The effect of maturity and depositional redox conditions on archael tetraether lipid palaeothermomtry. *Organic Geochemistry, 35*, 567-571.

Schouten, S., Hopmans, E.C., & Sinninghe Damsté, J.S. (2013). The organic geochemistry of glycerol dialkyl glycerol tetraether lipids: A review. *Organic Geochemistry, 54*, 19-61.

Shindell, D.T., Schmidt, G.A., Mann, M.E., Rind, D., & Waple, A. (2001). Solar forcing of regional climate change during the Maunder Minimum. *Science, 294*, 2159-2152.

Sicre, M.-A., Hall, I.R., Mignot, J., Khodri, M., Ezat, U., Truong, M.-X., Eiríksson, J., & Knudsen, K.-L. (2011). Sea surface temperature variability in the subpolar Atlantic over the last two millennia. *Paleoceanography, 26*, 1-10.

Sicre, M.-A., Khodri, M., Mignot, J., Eiríksson, J., Knudsen, K.-L., Ezat, U., Closset, I., Nogues, P., & Massé, G. (2013). Sea surface temperature and sea ice variability in the subpolar North Atlantic from explosive volcanism of the late thirteenth century. *Geophysical Research Letters, 40*, 5526-5539.

Slawinska, J., & Robock, A. (2018). Impact of volcanic eruptions on decadal to centennial fluctuations of Arctic sea ice extent during the last millennium and on initiation of the Little Ice Age. *Journal of Climate, 31*, 2145-2167.

Smik, L., Cabedo-Sanz, P., & Belt, S.T. (2016). Semi-quantitative estimates of paleo Arctic sea ice concentration based on source-specific highly branched isoprenoid alkenes: A further development of the PIP_{25} index. *Organic Geochemistry, 92*, 63-69.

Smith, L.M., Andrews, J.T., Castañeda, I.S., Kristjánsdóttir, G.B., Jennings, A.E., & Sveinbjörnsdóttir, Á.E. (2005). Temperature reconstructions for SW and N Iceland waters over the last 10 cal ka based on $\delta^{18}O$ records from planktic and benthic foraminifera. *Quaternary Science Reviews, 24*, 1723-1740.

Solignac, S., Giraudeau, J., & de Vernal, A. (2006). Holocene sea surface conditions in the western North Atlantic: Spatial and temporal heterogeneities. *Paleoceanography, 21*, 1-6.

Spielhagen, R.F., Werner, K., Sørensen, S.A., Zamelczyk, K., Kandiano, E., Budeus, G., Husum, K., Marchitto, T.M., & Hald, M. (2011). Enhanced modern heat transfer to the Arctic by warm Atlantic water. *Science, 311*, 450-453.

Stefánsson, U. (1962). North Icelandic Waters. *Rit Fiskideildar III. Bind, vol 3*.

Stefánsson, U. (1968). Dissolved nutrients, oxygen and water masses in the Northern Irminger Sea. *Deep-Sea Research, 15*, 541-575.

Stefánsson, U., & Ólafsson, J. (1991). Nutrients and fertility of Icelandic waters. *Rit fiskideildar*, 1-56.

Stein, R., Fahl, K., Schreck, M., Knorr, G., Niessen, F., Forwick, M., Gebhardt, C., Jensen, L., Kaminski, M., Kopf, A., Matthiessen, J., Jokat, W., & Lohmann, G. (2016). Evidence for ice-free summers in the late Miocene central Arctic Ocean. *Nature Communications, 7*, 11148.

Stuiver, M., Reimer, P.J., & Reimer, R.W. (2018). CALIB 7.1 [WWW program] at http://calib.org, accessed 2018-11-16.

Thornalley, D.J.R., Oppo, D.W., Ortega, P., Robson, J.I., Brierley, C.M., Davis, R., Hall, I.R., Moffa-Sanchez, P., Rose, N.L., Spooner, P.T., Yashayaev, I., & Keigwin, L.D. (2018). Anomalously weak Labrador Sea convection and Atlantic overturning during the past 150 years. *Nature, 556*, 227-232.

Thorndike, A.S., Rothrock, D.A., Maykut, G.A., & Colony, R. (1975). The thickness distribution of sea ice. *Journal of Geophysical Research, 80*, 4501-4513.

Tierney, J.E., Tingley, M.P., (2014). A Bayesian, spatially-varying calibration model for the TEX_{86} proxy. *Geochimica et Cosmochimica Acta, 127*, 83-106.

Trouet, V., Esper, J., Graham, N.E., Baker, A., Scourse, J.D., & Frank, D.C. (2009_. Persistent positive North Atlantic oscillation mode dominated the medieval climate anomaly. *Science, 324*, 78-80.

Volkman, J.K. (1986). A review of sterol markers for marine and terrigenous organic matter. *Organic Geochemistry, 9*, 83-99.

Volkman, J.K., Barrett, S.M., Blackburn, S.I., Mansour, M.P., Sikes, E.L., & Gelin, F. (1998). Microalgal biomarkers: a review of recent developments. *Organic Geochemistry, 29*, 1163-1179.

Wanamaker, A.D., Butler, P.G., Scourse, J.D., Heinemeier, J., Eiríksson, J., Knudsen, K.L., & Richardson, C.A. (2012). Surface changes in the North Atlantic meridional overturning circulation during the last millennium. *Nature Communications, 3*, 1-7.

Wuchter, C., Schouten, S., Coolen, M.J.L., & Sinninghe Damsté, J.S. (2004). Temperature-dependent variation in the distribution of tetraether membrane lipids of marine Crenarchaeota: implications for TEX_{86} paleothermometry. *Paleoceanography, 19*, 1-10.

Wuchter, C., Schouten, S., Wakeham, S.G., & Sinninghe Damsté, J.S. (2005). Temporal and spatial variation in tetraether membrane lipids of marine Crenarchaeota in particulate organic matter: implications for TEX_{86} paleothermometry. *Paleoceanography 20*, 1-11.

Wunsch, C. (1980). Meridional heat flux of the North Atlantic Ocean. *Proceedings of the National Academy of Sciences*, *77*, 5043-5047.

Xiao, X., Zhao, M., Knudsen, K.L., Sha, L., Eiríksson, J., Gudmundsdóttir, E., Jiang, H., & Guo, Z. (2017). Deglacial and Holocene sea-ice variability north of Iceland and response to ocean circulation changes. *Earth and Planetary Science Letters*, *472*, 14-24.

Zhai, L., Guðmundsson, K., Miller, P., Peng, W., Guðfinnsson, H., Debes, H., Hátun, H., White III, G.N., Hernández Walls, R., Sathyendranath, S., & Platt, T. (2012). Phytoplankton phenology and production around Iceland and Faroes. *Continental Shelf Research*, *37*, 15-25.

Zhong, Y., Miller, G.H., Otto-Bliesner, B.L., Holland, M.M., Bailey, D.A., Schneider, D.P., & Geirsdóttir, Á. (2010). Centennial-scale climate change from decadally-paced explosive volcanism: a coupled sea ice-ocean mechanism. *Climate Dynamics*, *37*, 2373-2387.

TABLES and FIGURES (8 units):

Table 1: Radiocarbon information. ^{14}C ages calibrated in Calib 7.1 (Stuiver et al., 2018) using the MARINE13 calibration curve (Reimer et al., 2013) and a ΔR of 0. Note that ^{14}C and calibrated ages are presented as BP (Before Present) in this table, and as CE (Common Era) in the main text.

Sediment core	Sediment depth (cm)	Lab ID	Material	δ^{13}C (‰)	Conventional ^{14}C date BP ± σ	ΔR	Calibrated age BP ± σ
B997-316 SGC	7.5	GRL-1691-S	mollusk (*T. equalis*)	0.62	294 ± 91	0	<400
B997-316 SGC	18	GRL-1690-S	mollusk (*T. equalis*)	-7.2	402 ± 38	0	<400
B997-316 GGC	49.5	CURL-18624	foraminifera (*N. labradorica* and *G. auriculata arctica)*	-14	1030 ± 15	0	600 ± 35
B997-316 GGC	135	CURL-19693	mollusk (*T. equalis*)	-9	1040 ± 15	0	620 ± 25
B997-316 GGC	160	CURL-19511	mollusk (*T. equalis*)	-8.5	1075 ± 15	0	645 ± 15
B997-316 GGC	212.5	CURL-20191	mollusk (*T. equalis*)	-5	1245 ± 15	0	780 ± 35

Table 2: Surface sediment calibration information. * indicates data from Rodrigo-Gámiz et al. (2015).

Site ID	Latitude	Longitude	Water depth (mbsl)	TEX_{86}^{L}
B997-313	66.617000°	-23.933000°	213	-0.67
B997-315	66.736000°	-24.332000°	217	-0.69
B997-316	66.746000°	-18.792000°	658	-0.68
B997-319	66.447000°	-18.843000°	422	-0.72
B997-324	66.527000°	-21.152000°	281	-0.65
B997-334	66.410000°	-21.880000°	112	-0.70
B997-329	65.965000°	-21.294000°	112	-0.68
B997-331	66.136000°	-21.591000°	165	-0.71
B997-344	64.836000°	-24.369000°	284	-0.61
B997-346	64.927000°	-24.129000°	320	-0.63

B997-347	63.928000°	-24.482000°	327	-0.64
Station 1*	62.000317°	-15.999183°	2255	-0.49
Station 7*	61.498550°	-24.172250°	1628	-0.51
Station 3*	63.366200°	-16.628267°	240	-0.59
Station 5*	63.583267°	-22.143733°	188	-0.62
Station 6*	63.238233°	-22.561417°	315	-0.61
Station 8*	64.293183°	-24.147083°	260	-0.62
Station 10*	66.677450°	-24.179500°	241	-0.64
Station 11*	66.633317°	-20.833433°	367	-0.63
Station 13*	67.501633°	-15.069217°	884	-0.71
Station 14*	66.303100°	-13.972817°	262	-0.68

Fig. 1: A) Overview maps of modern Icelandic oceanography. A) February 2014 and B) May 2014 50 m depth *in situ* temperature integrated from local CTD stations. Marine sediment cores (black dots) and used B997 surface sediment sample locations (black + and B997-316 GGC core site) are marked. C) May 2014 S-N trending cross section of NIS bathymetry and vertical *in situ* temperature structure along the Siglunes transect (A-A’ in panels A and B) and through the B997-316 GGC marine sediment core site. Data from Hafrannsóknastofnun (Marine and Freshwater Research Institute, http://www.hafro.is/Sjora/).

Fig. 2: CLAM age model. Gray shaded area denotes the 95% confidence envelope (Blaauw, 2010). Teal and asterisked mollusk ages are from the adjacent short gravity core, B997-316 SGC. Radiocarbon information provided in Table 1.

Fig. 3: B997-316 GGC marine sediment core climate proxies over the last millennium. A) % quartz, B) % calcite, C) triene Z concentrations, D) diene II concentrations, E) IP_{25} concentrations, and F) TEX_{86}^{L}. Blue boxes highlight colder, LIA-like conditions reflected in the surface climate proxies (A-E) and the subsurface proxy (F).

Fig. 4: Regression analysis summary of surface sediment GDGT calibration. A) Correlation coefficient (R^2) of all 21 surface sediment TEX_{86}^{L} values (Rodrigo-Gámiz et al., 2015; this study)

against seasonal and annual temperature depth integrations. B) Calibration of Icelandic marine surface sediment TEX_{86}^{L} values against winter 0-200 m temperature, where gray lines denote the 95% confidence envelope. Surface sediment data shown as closed circles (this study) and open circles (Rodrigo-Gámiz et al., 2015).

Fig. 5: Comparison of the available TEX_{86}^{L} temperature calibrations on the B997-316 GGC sediment record. Icelandic winter subsurface temperature (this study), annual SST (Kim et al., 2010) and annual subsurface temperature (Kim et al., 2012). Modern (1995-2004 CE) winter subsurface temperature at the B997-316 GGC site marked with gray dashed line (Locarnini et al., 2010).

Fig. 6: Comparison of select B997-316 GGC marine climate proxies to other well-dated Icelandic NIS marine climate records. A) B997-316 GGC IP_{25} concentrations (this study), B) triene Z concentrations (this study), C) MD99-2275 alkenone-inferred SST (Sicre et al., 2011), D) B997-316 GGC GDGT-inferred subsurface temperatures, with values below the record mean (4.34 ^{o}C) highlighted in blue (this study), and E) schlerochronological ΔR record, where increases in ΔR_{shell} values reflect the incursion of older, Arctic waters (Wanamaker et al., 2012). Vertical yellow bars highlight the period of interpreted thick sea ice, and the associated insulation/warming of the subsurface. Dashed blue lines bound the inferred periods of LIA-like conditions for the surface (A-C) and subsurface (D).

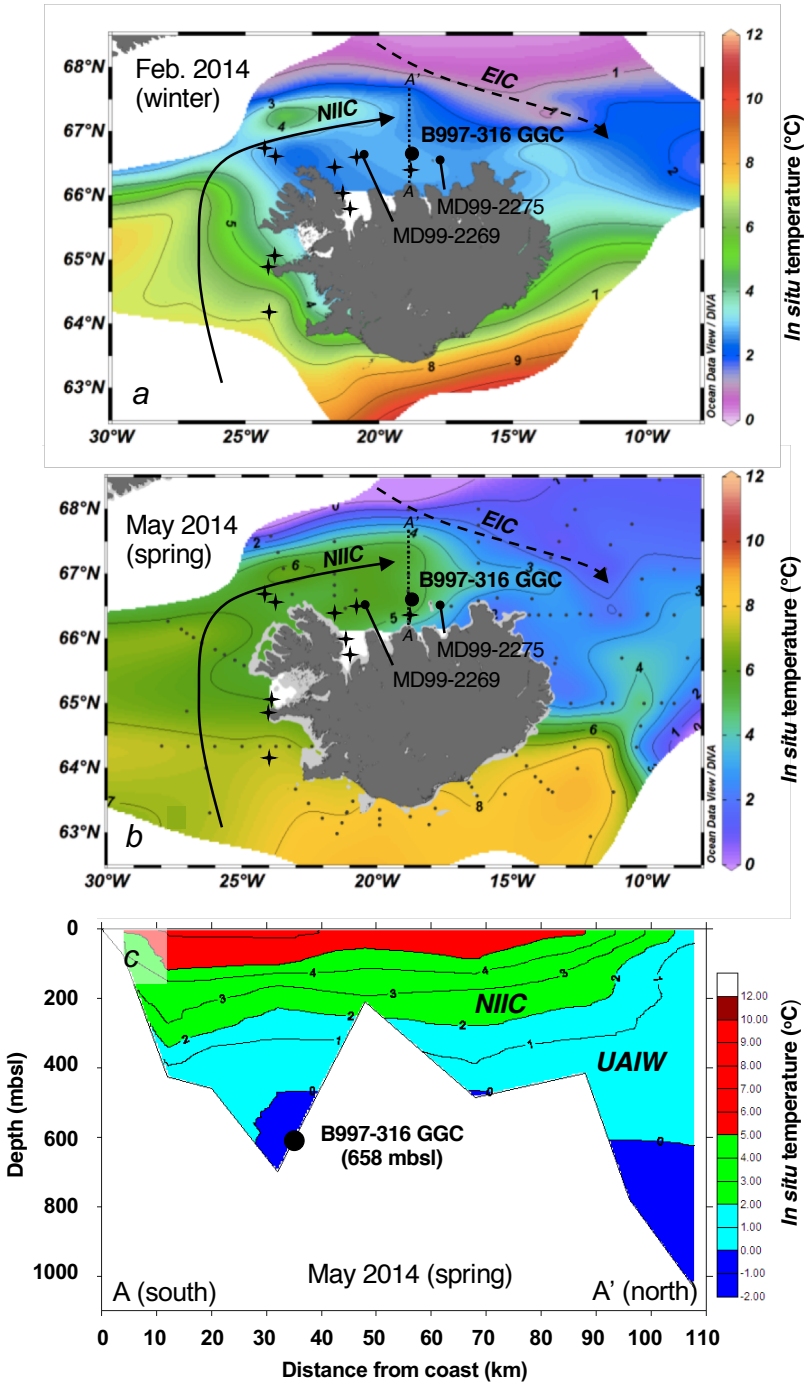

Fig. 1: A) Overview maps of modern Icelandic oceanography. A) February 2014 and B) May 2014 50 m depth potential temperature integrated from local CTD stations. Marine sediment cores (black dots) and used B997 surface sediment sample locations (black + and B997-316 GGC core site) are marked. C) May 2014 S-N trending cross section of NIS bathymetry and vertical potential temperature structure along the Siglunes transect and through the B997-316 GGC marine sediment core site. Data from Hafrannsóknastofnun (Marine and Freshwater Research Institute, http://www.hafro.is/Sjora/).

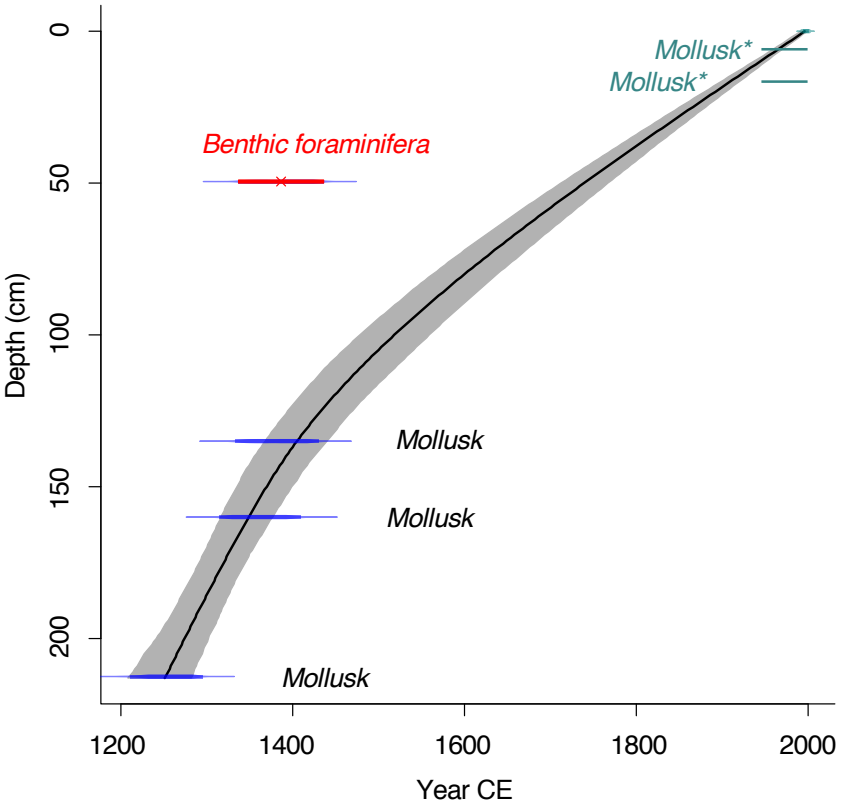

Fig 2: CLAM age model. Gray shaded area denotes the 95% confidence envelope (Blaauw, 2010). Teal and asterisked mollusk ages are from the adjacent short gravity core, B997-316 SGC, and not used as age control points in this model. Radiocarbon information provided in Table 1.

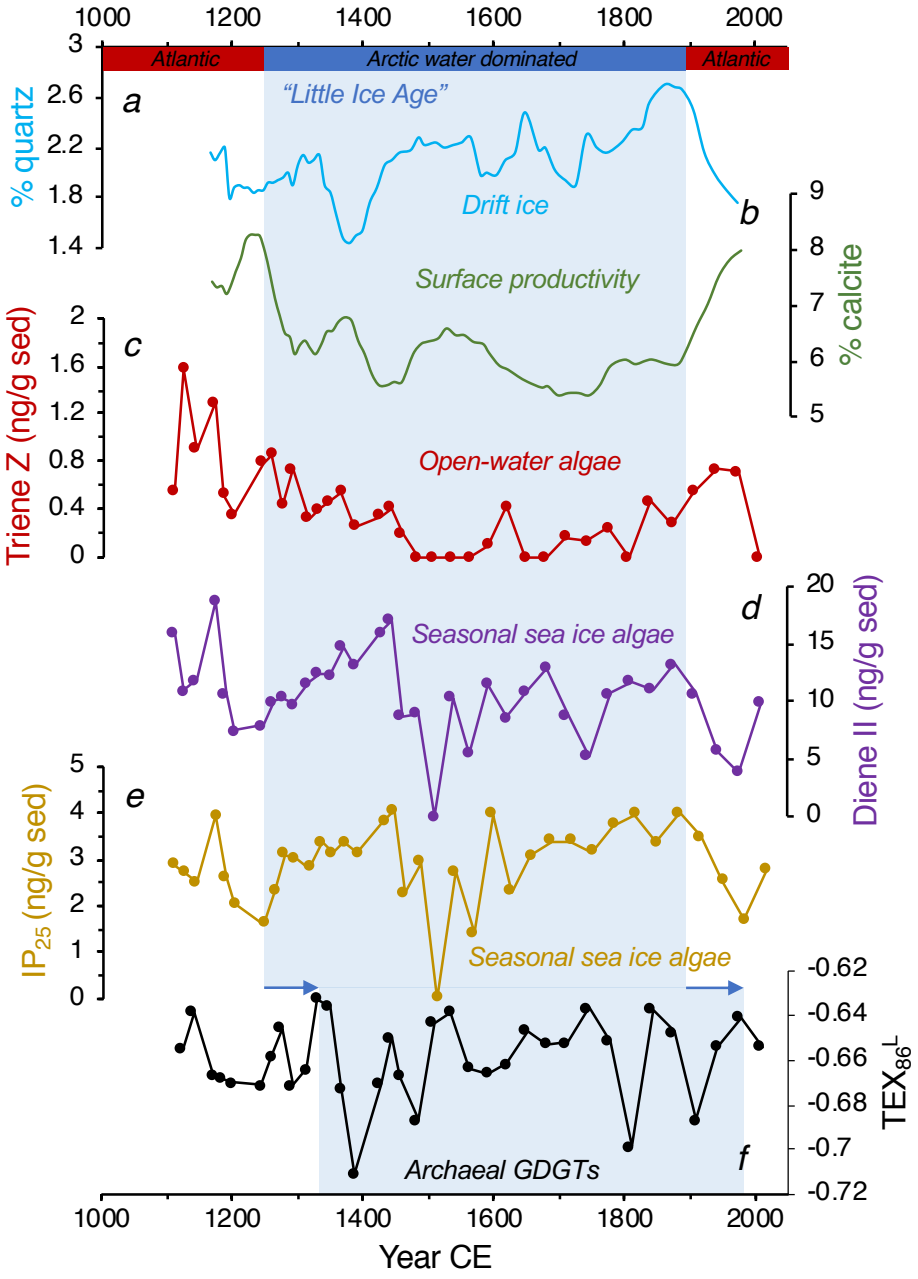

Fig. 3: B997-316 GGC marine sediment core climate proxies over the last millennium. A) % quartz, B) % calcite, C) triene Z concentrations, D) diene II concentrations, E) IP_{25} concentrations, and F) TEX_{86}^{L}. Blue boxes highlight colder, LIA-like conditions reflected in the surface climate proxies (A-E) and the subsurface proxy (F).

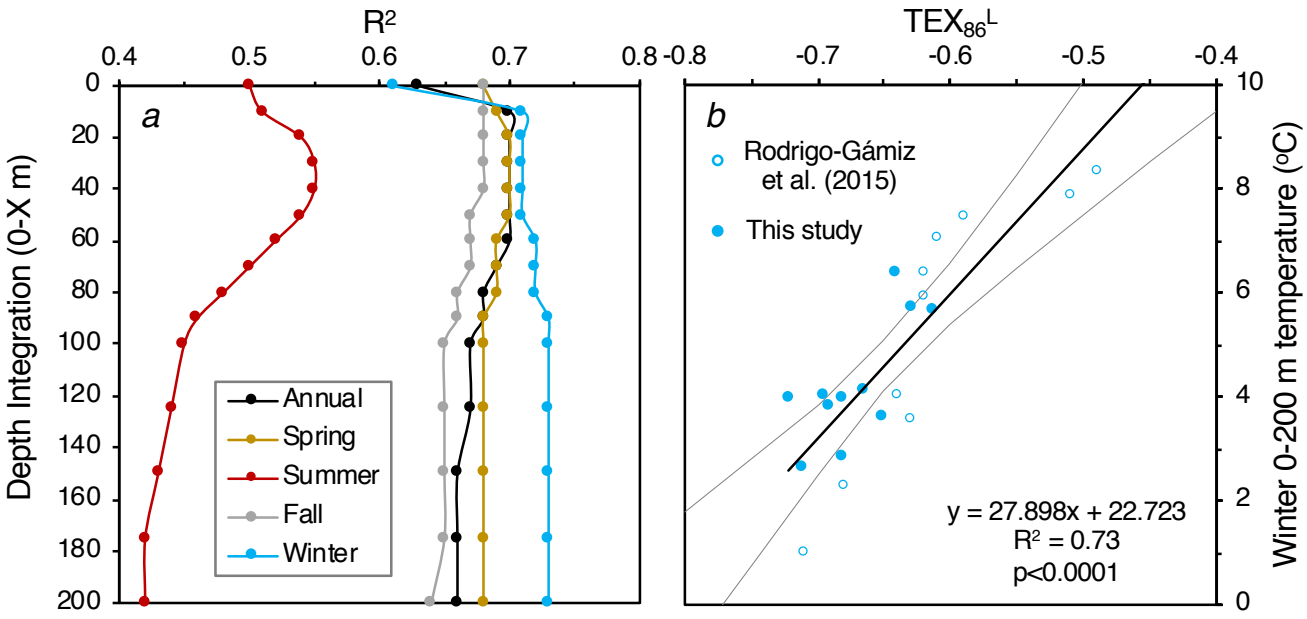

Fig. 4: Regression analysis summary of surface sediment GDGT calibration. A) Correlation coefficient (R^2) of all 21 surface sediment TEX_{86}^L values against seasonal and annual temperature depth integrations. B) Calibration of Icelandic marine surface sediment TEX_{86}^L values against winter 0-200 m temperature, where gray lines denote the 95% confidence envelope. Surface sediment data shown as closed circles (this study) and open circles (Rodrigo-Gámiz et al., 2015).

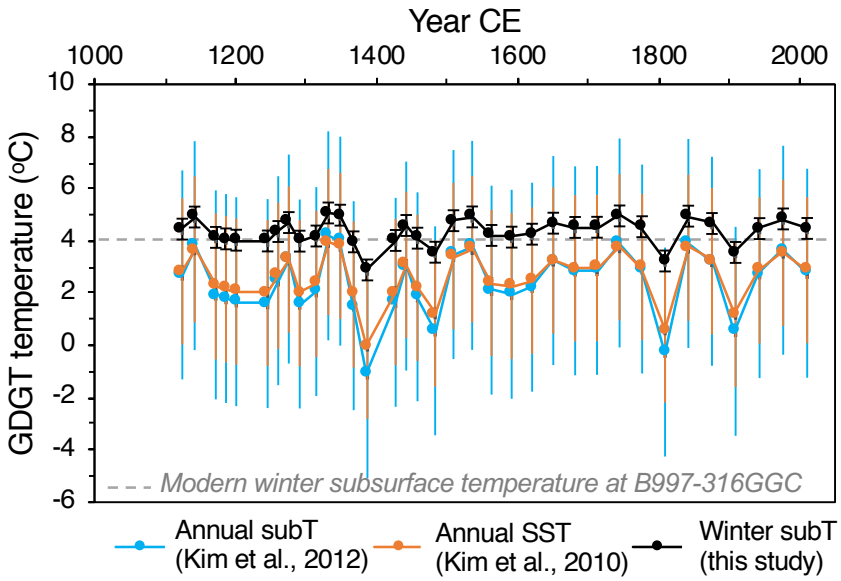

Fig. 5: Comparison of the available TEX_{86}^{L} temperature calibrations on the B997-316 GGC sediment record. Icelandic winter subsurface temperature (this study), annual SST (Kim et al., 2010) and annual subsurface temperature (Kim et al., 2012). Modern winter subsurface temperature at the B997-316 GGC site marked with gray dashed line.

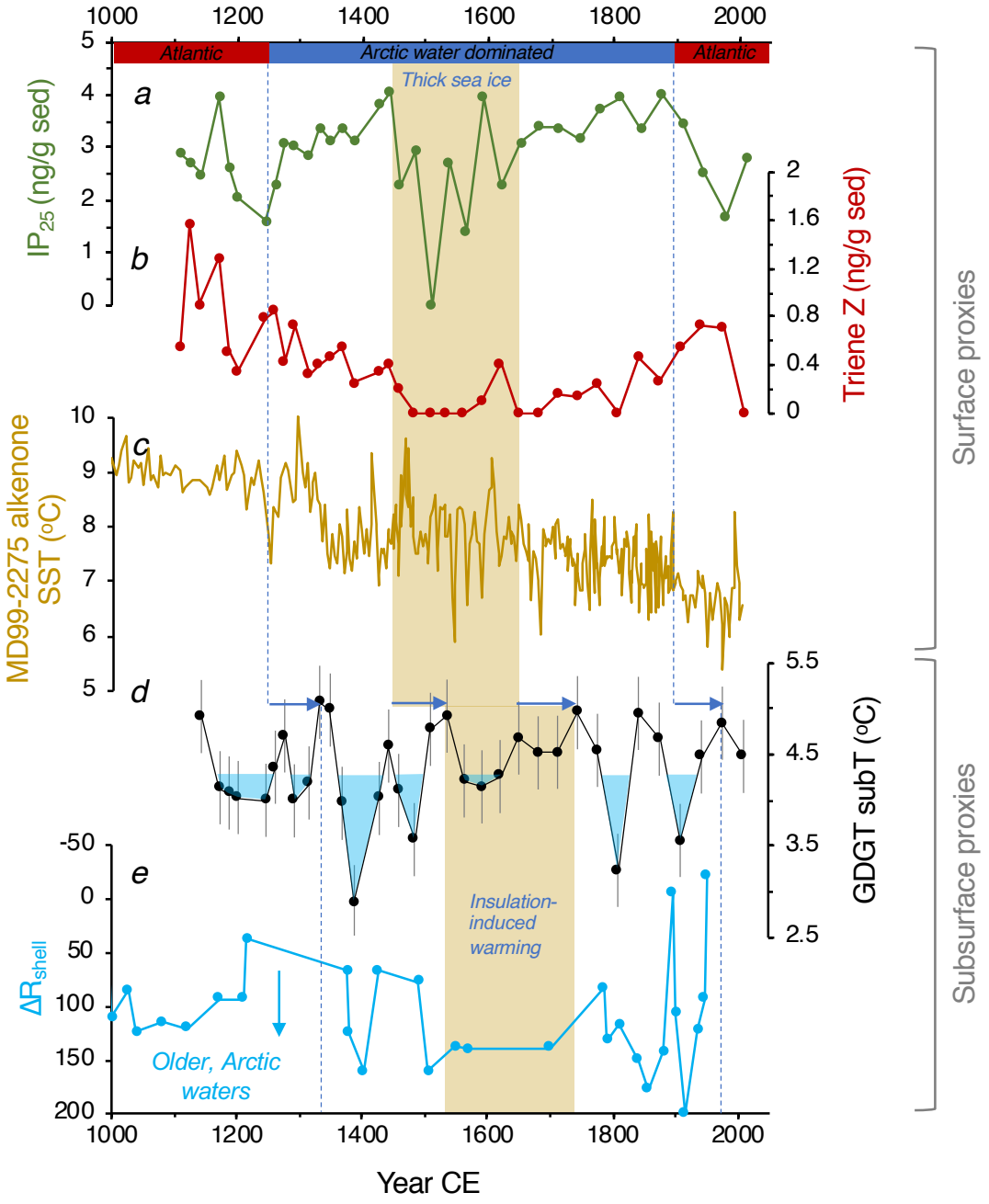

Fig. 6: Comparison of select B997-316 GGC marine climate proxies to other well-dated, high-resolution Icelandic NIS marine climate records. A) B997-316 GGC IP_{25} concentrations (this study), B) Triene Z concentrations (this study), C) MD99-2275 alkenone-inferred SST (Sicre et al., 2011), D) B997-316 GGC GDGT-inferred subsurface temperatures, with values below the record mean highlighted in blue (this study), and E) schlerochronological ΔR record, where increases in ΔR_{shell} values reflect the incursion of older, Arctic waters, and a weaker AMOC (Wanamaker et al., 2012). Vertical yellow bars highlight the period of interpreted thick sea ice, and then the delayed associated insulation/warming of the subsurface. Dashed blue lines bound the inferred periods of LIA-like conditions for the surface (A-C) and subsurface (D) proxies.

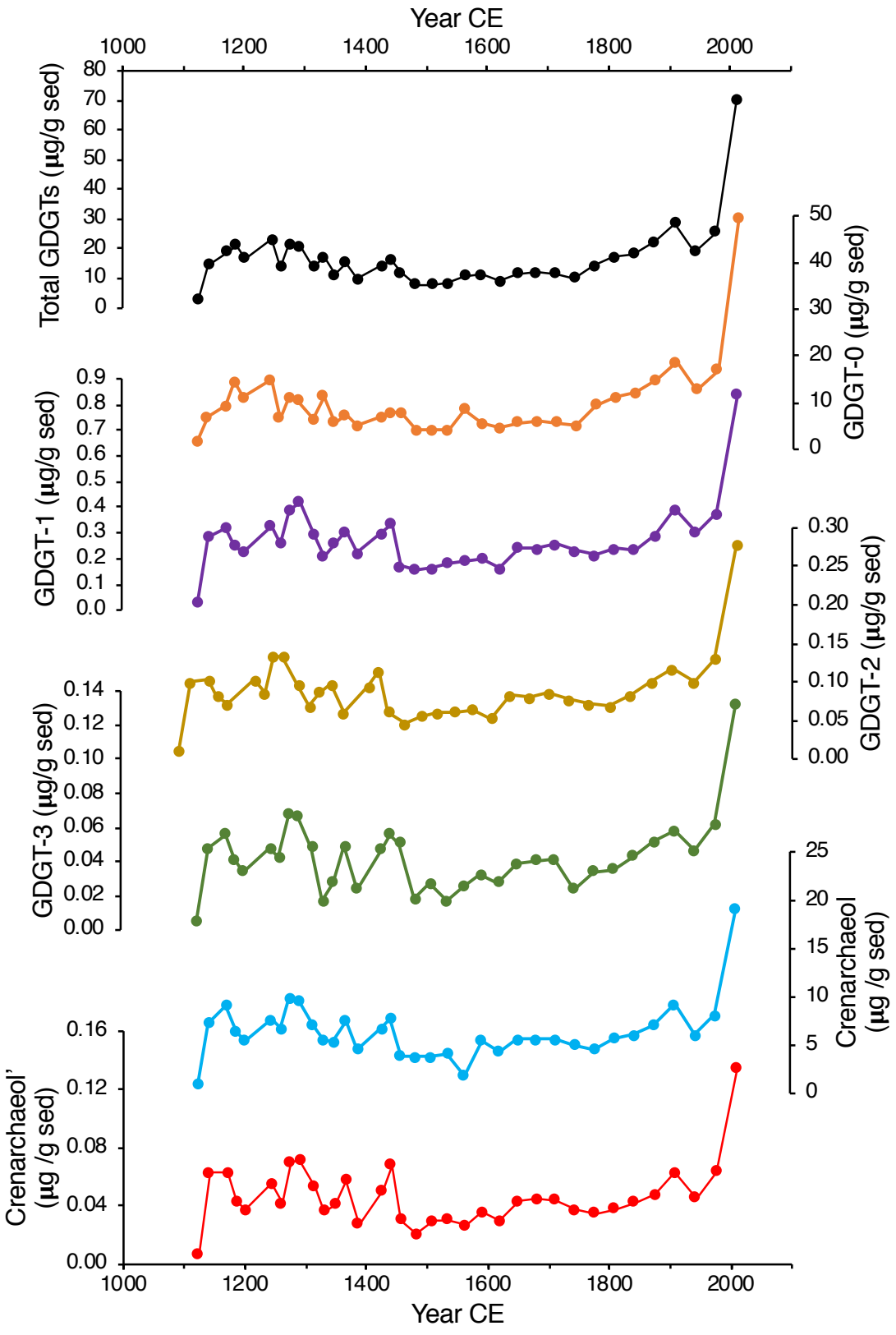

Supplemental Fig S1: GDGT concentrations in B997-316 GGC marine sediment samples.

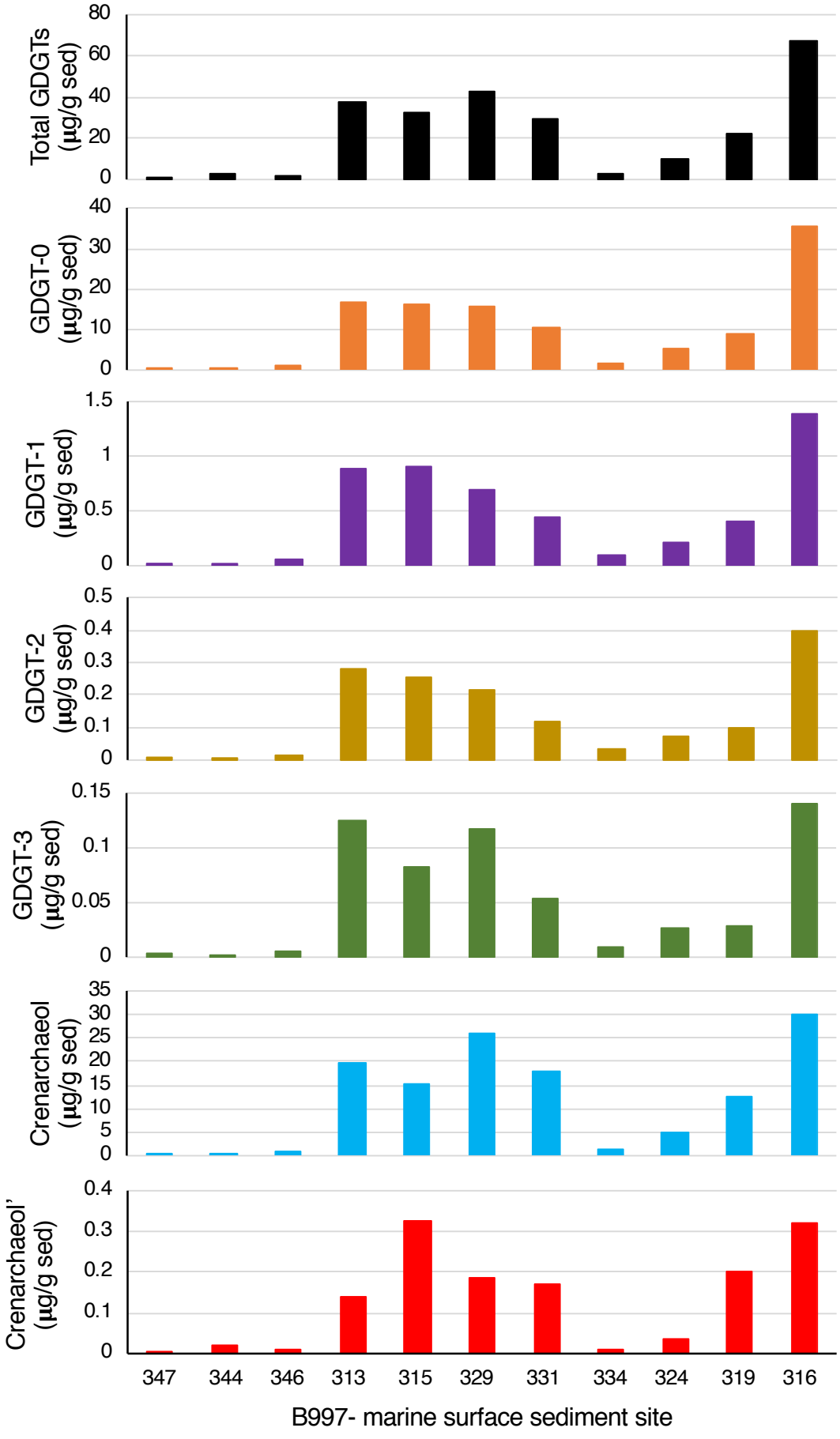

Supplemental Fig S2: GDGT concentrations in B997 marine surface sediment samples. Sample labels are abbreviated (i.e., 347 = B997-347) and ordered geographically from the southwestern-most (347, left) to the northeastern-most (316, right).

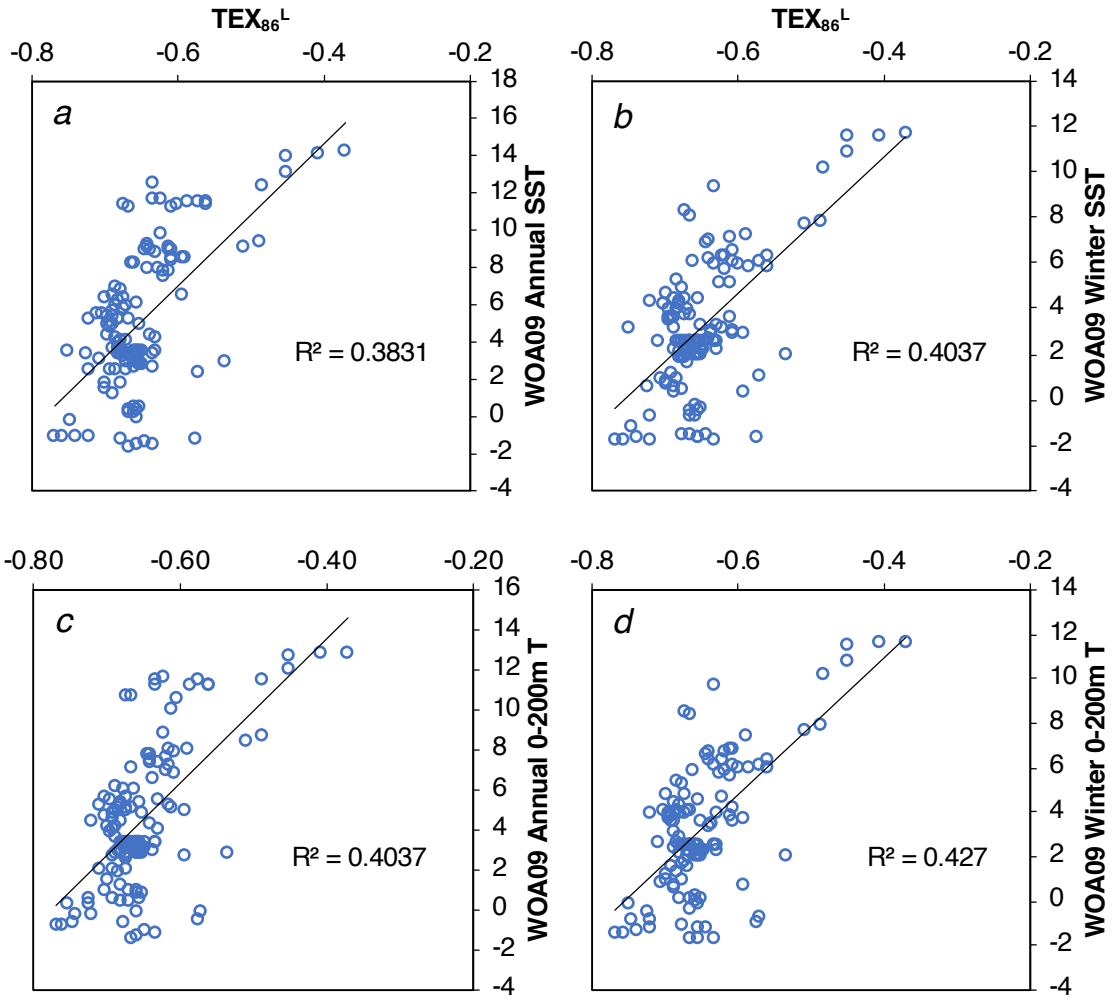

Supplemental Fig S3: Using samples selected from the global calibration of Kim et al. (2010) we tested whether we could improve the local calibration by extending the range of samples, and thus, the environmental gradient. A) Annual SST, B) Winter SST, C) Annual 0-200 m T, and D) 0-200m T. Panel E highlights the northern hemisphere samples included from the the global calibration of Kim et al. (2010).